Agricultural Water Management 283 (2023) 108319

Contents lists available at ScienceDirect

Agricultural Water Management

journal homepage: www.elsevier.com/locate/agwat

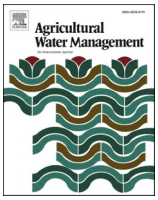

Water use, soil water balance and soil salinization risks of Mediterranean tree orchards in southern Portugal under current climate variability: Issues for salinity control and irrigation management

Tiago B. Ramos [a,*], Hanaa Darouich [b], Ana R. Oliveira [a], Mohammad Farzamian [c], Tomás Monteiro [d], Nádia Castanheira [c], Ana Paz [c], Carlos Alexandre [d], Maria C. Gonçalves [c], Luís S. Pereira [b]

[a] Centro de Ciência e Tecnologia do Ambiente e do Mar (MARETEC–LARSyS), Instituto Superior Técnico, Universidade de Lisboa, Av. Rovisco Pais, 1, 1049-001 Lisboa, Portugal
[b] LEAF – Linking Landscape, Environment, Agriculture and Food Research Center, Associated Laboratory TERRA, Instituto Superior de Agronomia, Universidade de Lisboa, Tapada da Ajuda, 1349-017 Lisboa, Portugal
[c] Instituto Nacional de Investigação Agrária e Veterinária, Avenida da República, Quinta do Marquês, 2780-157 Oeiras, Portugal
[d] MED – Mediterranean Institute for Agriculture, Environment and Development, University of Évora, Pólo da Mitra, Apartado 94, 7006-554 Évora, Portugal

ARTICLE INFO

Handling Editor: Dr R Thompson

Keywords:
Irrigation water management
HYDRUS-1D
Leaching needs
Salinity build-up
Solute stress

ABSTRACT

Secondary salinization has long been reported in the Roxo irrigation district (RID), southern Portugal, due to the use of saline-prone irrigation water and the existence of poorly structured soils. This study assessed the soil water and salt budgets in nine commercial orchards located in the RID using the multiple ion chemistry module available in the HYDRUS-1D model during the 2019 and 2020 growing seasons. The studied crops were almond, olive, citrus (orange, mandarin, and clementine), and pomegranate. The model successfully simulated soil water contents measured in the different fields but there was a clear underestimation of the electrical conductivity of the soil saturation paste extract (EC_e) in some locations, while simulations of the sodium adsorption ratio (SAR) were generally acceptable. Modeling errors were mostly associated with missing information on fertigation events rather than related to the effects of irrigation water quality. The water and salt balances were also computed for the 1979–2020 period. Considering the probability of non-exceedance of salt accumulation during this period, the risk of salinity build-up was high to very high for the very dry years in most fields, except in the citrus sites. The factors influencing the salt accumulation were the irrigation strategy, the seasonal irrigation and rainfall depths, the duration of the crop growth period, the rainfall distribution in the late and non-growing stages, the soil drainage conditions, and the irrigation water quality. For the current climate conditions and irrigation water quality, the risk of soil salinity levels affecting crop development and yields was found to be minor. This means that, despite salts tended to accumulate in the rootzone over a season, under current conditions the salinity stress did not reach harmful levels for plants. Only in two of the study sites, there was a need to promote salt leaching. Hence, this study shows that soil salinization risks in the study area are low but, for given locations during drier seasons, there is a need for tailored irrigation solutions aimed at the conservation of soil and water resources.

1. Introduction

Agriculture, and irrigation in particular, is responsible for 70% of all freshwater withdrawals in the world and 90% in the least developed regions (UNESCO, 2020). With diverted water, farmers can fulfill crop water requirements, diversify crop production, increase food production, meet the growing food demand, ensure food stability, and increase their income and prosperity of rural areas (Pereira et al., 2002, 2009). The downside is the widespread degradation of soil and water resources, particularly in water-scarce regions, due to poor management of irrigation water. In these regions, mostly characterized by arid to dry sub-humid climates, secondary human-induced soil salinization assumes

* Correspondence to: MARETEC–LARSyS, Instituto Superior Técnico, Av. Rovisco Pais, 1049-001 Lisbon, Portugal.
E-mail addresses: tiagobramos@tecnico.ulisboa.pt, tiago_ramos@netcabo.pt (T.B. Ramos).

https://doi.org/10.1016/j.agwat.2023.108319
Received 25 January 2023; Received in revised form 31 March 2023; Accepted 17 April 2023
Available online 23 April 2023

major relevancy, with recent estimates of 30% of irrigated lands as salt-affected (Hopmans et al., 2021).

Secondary salinization is mainly caused by poor management of irrigation water, including the use of non-conventional water resources and of fertilizers and other chemicals, and changes in land use (Rhoades et al., 1992; Hoffman and Shalhevet, 2007; Pereira et al., 2014; Minhas et al., 2020). Factors contributing to secondary salinization consist of high evapotranspiration and soil and groundwater conditions favoring soil water dynamics and solute transport, i.e., climate conditions, soil properties, irrigation method, and associated soil and water management practices (Hopmans et al., 2021). Irrigation management strategies to cope with soil salinity were recently reviewed by Minhas et al. (2020), where the need to prevent the build-up of salts in the root zone to levels that limit the root water uptake were emphasized. Controlling the salt balances in the soil-water system by preventing accumulation in the root zone, and minimizing the damaging effect of salinity on crop transpiration and soil evaporation for optimal crop growth were duly considered.

The current study develops in the Roxo irrigation district (RID), in Alentejo, southern Portugal, and follows a companion paper dealing with assessing irrigation and determining the crop coefficients to support irrigation scheduling (Ramos et al., 2023). Both studies result from the need to increase knowledge on the water use and environmental impacts in the orchard systems currently dominating the landscape in Alentejo. The region has faced significant changes in the landscape over the last decade where the traditional crops, irrigated and rainfed cereals, were abruptly replaced by orchards, mainly olive and almond. These orchards mostly are of high ($\geq$300 trees ha^{-1}) and very high-density ($\geq$1500 trees ha^{-1}), which require high and precise input factors (Paço et al., 2019). While some studies already exist to address improved crop water use (Paço et al., 2019, 2014; Conceição et al., 2017; Santos, 2018) and prevention of non-point source pollution due to fertigation practices (Cameira et al., 2014), these stress the need to further gain knowledge on crop water use that control environmental impacts.

The RID has also been historically the center of soil salinization problems in southern Portugal resulting from the semi-arid climate, the use of poor-quality irrigation water, and the use of soils for irrigation with deficient drainage conditions, namely Stagnic Luvisols and Planosols (Martins et al., 2005; Alexandre et al., 2018). While irrigation water quality problems were attenuated after 2016 with the connection of the RID to the Alqueva system, deficient soil drainage conditions remained the same in most of the area. On the other hand, soil salinization risks may have likely been aggravated due to less percolating water resulting from a decreasing rainfall trend as reported by Portela et al. (2020).

Ramos et al. (2023), in the companion paper, evaluated the water use and water balance resulting from current irrigation management in some of the most representative orchard systems in the RID using the FAO-56 dual crop coefficient approach (Allen et al., 1998, 2005) and the SIMDualKc model (Rosa et al., 2012). That study showed that mild water deficit irrigation schedules are viable, which can lead to significant water savings in the region. The study further made clear the need for better training farmers relative to irrigation water management, including in their computing skills, and that support on the various orchard management issues, namely relative to water and fertility, become available, thus contributing to better facing global change challenges. This companion paper now focuses on the quantitative evaluation of soil salinization risks resulting from current irrigation management and climate conditions.

The major ion chemistry module in the HYDRUS-1D software package (Šimůnek et al., 2008, 2016) was the tool of choice. The reasons for choosing this model were various. Firstly, the capacity of HYDRUS-1D for considering multicomponent solute transport, being able to describe the subsurface transport of multiple ions that may mutually interact, create various complex species, compete for sorption sites, and/or precipitate or dissolve (Šimůnek et al., 2016), thus showing a more realistic approach to the salinization problem than the simple modeling of the electrical conductivity of the soil solution as a non-reactive tracer. Secondly, the capacity of defining the atmospheric boundary conditions in the case study sites by adopting the estimated potential transpiration and soil evaporation fluxes from the companion paper (Ramos et al., 2023), allowing thus a more accurate representation of evapotranspiration fluxes in rather complex agricultural systems. Thirdly, the extensive calibration/validation of model simulations already performed in the region (Gonçalves et al., 2006; Ramos et al., 2011), as well as its use for assessment of soil salinization and sodification risks under different scenarios related to irrigation management, water quality, and climate change (Ramos et al., 2019). Lastly, the considerable number of simulations needed for this study, with HYDRUS-1D providing fast and reliable estimates of soil salinization and sodification risks in the long-term despite using a simpler representation of the modeling system when compared with the two- and three-dimensional HYDRUS versions (Ramos et al., 2019).

The objectives of this study, therefore, were: (i) to calibrate and validate the HYDRUS-1D model in various almond, olive, citrus (orange, clementine, mandarin), and pomegranate orchards of Alentejo using field data of the 2019 and 2020 growing seasons; (ii) to evaluate the components of the soil water and salt balances relative to current irrigation management; and, (iii) to quantify soil salinization risks and leaching needs in the different study sites in a climate variability context using data from 1979 to 2020. As such, this study complements the one reported in the companion paper (Ramos et al., 2013) by further contributing to improve irrigation water use in the Alentejo region considering the sustainability of local soil and water resources and response of local production systems to climate variability.

2. Material and methods

2.1. Description of the case studies

This study was carried out in nine commercial orchards located in the RID, Montes Velhos, Aljustrel, Portugal, and developed from January 1st, 2019 to December 31st, 2020 (Fig. 1). The climate is semi-arid, with the mean air temperature ranging from 9.8ºC in January to 23.1ºC in August. The mean annual rainfall sums 454 mm, mostly occurring from October to May. The mean annual reference evapotranspiration (ET_o) computed with the FAO Penman-Monteith (PM) equation (Allen et al., 1998) sums 1363 mm (1979–2020). The weather data during the study period (2019–2020) were collected at the local meteorological station. Fig. 2 shows the information of interest to this study, namely the daily values of the ET_o and rainfall.

The studied crops were almond (*Prunus amygdalus* Batsch), olive (*Olea europaea* L.), citrus (*Citrus* spp.), and pomegranate (*Punica granatum* L.), covering the most representative perennials grown in the region. In five locations, orchards were on ridges, mostly trapezoidal shaped with 0.25–0.70 m height, and 1.2–1.6 m wide at the top and 2.3–2.8 m wide at the bottom. Table 1 presents the main characteristics of the selected orchards, including location, crop variety, crop density, training system, and soil type. The main physical and chemical properties of soils in the nine study sites are given in Table 2. The methodologies used in the respective soil analyses can be found in the companion paper (Ramos et al., 2023). In all sites, the groundwater table was below 5.5 m.

Orchards were drip irrigated, with irrigation scheduling decided by farmers and following standard practices in the region. Daily irrigation depths averaged between 2.7 mm in the orange (P6) and 7.4 mm in the mandarin (P8) fields. The season irrigation depths averaged 658 mm in almond, 320 mm in olive, 830 mm in citrus, and 791 mm in pomegranate. Soil water contents were continuously monitored at depths of 0.1, 0.3, 0.5, and 0.7 m using EnviroPro MT capacitance probes (MAIT Industries, Australia) installed in the crop rows as detailed in the companion paper (Ramos et al., 2023). The electrical conductivity of the soil saturation paste extract (EC_e) was periodically measured in disturbed

Fig. 1. Location of the study sites.

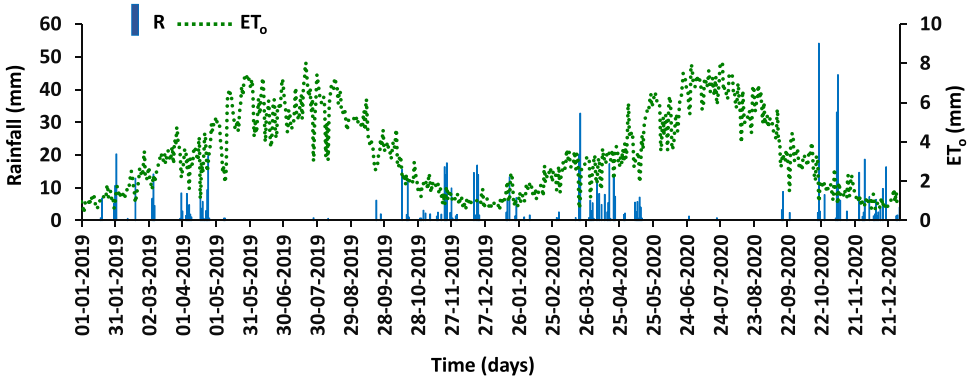

Fig. 2. Rainfall (R) and reference evapotranspiration (ET_o) in the study area during 2019 and 2020.

Table 1
Location and general characteristics of the case studies.

Field plot	Crop	Variety	Latitude	Longitude	Density (trees ha^{-1})	Soil classification*	Slope (%)	Ridges
P1	Almond	Monterey	37.9387	-8.1525	391	Chromic Abruptic Luvisol	5.0	No
P2	Almond	Monterey	37.9407	-8.1536	391	Chromic Abruptic Luvisol	5.0	No
P3	Olive	Arbequina	37.9407	-8.1419	319	Chromic Dystric Cambisol	< 1.0	Yes
P4	Olive	Cobrançosa	37.9512	-8.1538	297	Chromic Dystric Cambisol	< 1.0	No
P5	Olive	Picual	37.9540	-8.1398	297	Calcaric Regosol	1.0 – 2.0	No
P6	Orange	Fukumoto	37.9700	-8.1808	404	Chromic Abruptic Luvisol	1.0 – 2.0	Yes
P7	Clementine	Oronules	37.9697	-8.1758	675	Eutric Sodic Stagnic Regosol	< 1.0	Yes
P8	Mandarin	Setubalense	37.9675	-8.1808	529	Eutric Sodic Regosol	< 1.0	Yes
P9	Pomegranate	Acco	37.9644	-8.1841	666	Luvic Planosol	< 1.0	Yes

Note: * According to IUSS Working Group (2014).

soil samples collected below emitters (U.S. Salinity Laboratory Staff, 1954), at depths of 0.0–0.2, 0.2–0.4, 0.4–0.6, and 0.6–0.8 m, using an auger (two locations per site). The electrical conductivity of irrigation water (EC_{iw}) was periodically monitored in the RID irrigation channel, with values averaging 0.72 dS m^{-1}, which contrast with the previous range of values (1.05–1.67 dS m^{-1}) measured in the RDI channels between 2003 and 2006 (Martins et al., 2005) before the RDI system was connected to the Alqueva system. The concentration of Ca^{2+}, Mg^{2+}, Na^{+}, and K^{+} in the irrigation water averaged 2.10, 2.50, 2.32, and 0.05 mmol$_{(c)}$ L^{-1}, respectively.

Table 2
Main soil physical and chemical properties in the case studies.

Depth (m)	Soil texture				OM (%)	ρ_b (Mg m^{-3})	θ_S (cm^3 cm^{-3})	Soil hydraulic properties				EC_e (dS m^{-1})	SAR (mmol$_{(c)}$ l^{-1})$^{0.5}$
	CS (%)	FS (%)	Si (%)	C (%)				$\theta_{-10\ kPa}$ (cm^3 cm^{-3})	$\theta_{-100\ kPa}$ (cm^3 cm^{-3})	$\theta_{-1500\ kPa}$ (cm^3 cm^{-3})	K_s (cm d^{-1})		
P1. Almond													
0.0–0.3	46.0	23.7	15.4	14.9	2.2	1.33	0.419	0.225	0.149	0.067	172.2	0.21	1.47
0.3–0.5	35.2	16.6	13.2	35.0	0.8	1.41	0.388	0.215	0.146	0.135	75.2	0.29	1.07
0.5–1.0	27.6	13.1	13.1	46.2	0.4	-	-	-	-	-	-	0.34	1.52
P2. Almond													
0.0–0.2	41.0	28.0	17.1	13.9	2.0	1.48	0.418	0.195	0.135	0.080	90.8	0.20	2.08
0.2–0.4	27.8	20.0	13.4	38.8	1.1	1.41	0.421	0.202	0.171	0.080	90.8	0.18	2.73
0.4–0.7	12.5	20.5	12.0	55.0	0.8	-	-	-	-	-	-	0.19	3.96
0.7–1.0	35.5	31.8	15.9	16.8	-	-	-	-	-	-	-	0.47	4.84
P3. Olive													
0.0–0.4	19.9	38.7	21.1	20.3	1.2	1.34	0.458	0.198	0.135	0.105	73.4	0.20	0.99
0.4–0.6	21.9	33.9	21.5	22.7	1.0	-	-	-	-	-	-	0.14	0.83
0.6–0.8	23.8	31.9	19.2	25.1	0.6	-	-	-	-	-	-	0.23	0.82
P4. Olive													
0.0–0.4	27.1	38.5	17.7	16.7	2.6	1.36	0.409	0.192	0.132	0.075	83.8	0.20	0.80
0.4–0.7	27.3	19.1	10.2	43.4	0.7	-	-	-	-	-	-	0.10	1.15
0.7–1.0	32.0	10.6	7.5	49.9	1.7	-	-	-	-	-	-	0.26	1.67
P5. Olive													
0.0–0.5	15.7	16.4	20.0	48.0	1.5	1.38	0.543	0.469	0.403	0.295	500.0	0.24	0.56
0.5–0.8	29.6	20.0	22.5	27.9	0.3	-	-	-		-	-	0.22	0.79
P6. Orange													
0.0–0.7	39.4	34.5	13.1	13.0	0.9	1.50	0.409	0.252	0.186	0.100	451.0	0.51	2.65
0.7–0.9	28.2	23.8	14.9	33.1	3.8	-	-	-	-	-	-	0.33	4.93
P7. Clementine													
0.0–0.8	46.3	36.7	8.0	9.0	0.8	1.61	0.372	0.187	0.116	0.042	171.0	1.04	5.47
0.8–1.0	33.4	27.0	7.8	31.8	0.4	-	-	-	-	-	-	0.61	9.10
P8. Mandarin													
0.0–0.8	31.0	39.9	14.9	14.2	0.5	1.84	0.384	0.256	0.197	0.097	66.0	0.68	2.93
0.8–1.0	36.0	32.2	6.4	25.4	0.2	-	-	-	-	-	-	0.61	5.40
P9. Pomegranate													
0.0–0.6	49.6	37.6	7.2	5.6	1.5	1.51	0.382	0.195	0.125	0.045	132.5	0.38	2.79
0.6–0.8	44.1	31.2	7.3	17.4	1.4	-	-	-	-	-	-	0.17	3.85
0.8–1.0	42.5	37.1	6.9	13.5	0.5	-	-	-	-	-	-	0.13	5.40

Note: CS, coarse sand (2000–200 μm); FS, fine sand (200–20 μm); Si, silt (20–2 μm); C, clay (< 2 μm); ρ_b, soil bulk density; OM, soil organic matter; θ_S, soil water contents at saturation; $\theta_{-10\ kPa}$, $\theta_{-33\ kPa}$, $\theta_{-1585\ kPa}$, soil water contents − 10, − 100, and − 1500 kPa matric potential, respectively; K_s, saturated hydraulic conductivity; EC_e, electrical conductivity of the saturation paste extract; SAR, sodium adsorption ratio.

2.2. Modeling approach

2.2.1. Model description

The HYDRUS-1D software package (Šimůnek et al., 2016) was used to numerically simulate one-dimensional water flow and solute transport in variably-saturated porous media by solving the Richards and Fickian-based convection–dispersion equations, respectively, as follows:

$$\frac{\partial \theta}{\partial t} = \frac{\partial}{\partial z}\left[K(h)\left(\frac{\partial h}{\partial z} + 1\right)\right] - S(h, z, t) \tag{1}$$

$$\frac{\partial \theta c_k}{\partial t} + \rho \frac{\partial \bar{c}_k}{\partial t} = \frac{\partial}{\partial z}\left(\theta D \frac{\partial c_k}{\partial z}\right) - \frac{\partial q c_k}{\partial z} \tag{2}$$

where θ is the volumetric soil water content (L^3L^{-3}), t is time (T), z is the vertical space coordinate (L), h is the soil matric potential or pressure head (L), K is the hydraulic conductivity (LT^{-1}), S is the sink term accounting for water uptake by plant roots ($L^3L^{-3}T^{-1}$), c and $\bar{c}$ are solute concentrations in the liquid (ML^{-3}) and solid (MM^{-1}) phases, respectively, ρ is the soil bulk density (ML^{-3}), q is the volumetric flux density (LT^{-1}), D is the hydrodynamic dispersion coefficient (L^2T^{-1}), and subscript k represents the major cations present in our study (Na^+, Ca^{2+}, Mg^{2+}, and K^+). In this study, the major ion chemistry module was used for the computation of solute transport (Šimůnek and Suarez, 1997; Šimůnek et al., 2013), and no passive or active uptake of soil cations by plants was considered.

The unsaturated soil hydraulic properties were described using the van Genuchten–Mualem functional relationships (Mualem, 1976; van Genuchten, 1980):

$$S_e(h) = \frac{\theta(h) - \theta_r}{\theta_s - \theta_r} = \frac{1}{(1 + |\alpha h|^{\eta})^m} \tag{3}$$

$$K(h) = K_s S_e^{\ell}\left[1 - \left(1 - S_e^{1/m}\right)^m\right]^2 \tag{4}$$

where S_e is the effective saturation (-), θ_r and θ_s are the residual and saturated water contents (L^3L^{-3}), respectively, K_s is the saturated hydraulic conductivity (LT^{-1}), α (L^{-1}) and η (-) are empirical shape parameters, ℓ is a pore connectivity/tortuosity parameter (-), and m= 1–1/η.

The sink term S in the flow equation was computed according to the macroscopic approach introduced by Feddes et al. (1978), where the potential root water uptake rate, i.e., the potential crop transpiration rate (T_c), is distributed over the root zone and reduced due to the presence of depth-varying water and salinity stressors (Skaggs et al., 2006b; Šimůnek and Hopmans, 2009). The water stress response function was defined according to Feddes et al. (1978), in which root water uptake is at the potential rate when h is between h_2 and h_3, drops off linearly when $h > h_2$ or $h < h_3$, and becomes zero when $h < h_4$ or $h > h_1$ (subscripts 1–4 denote different threshold pressure heads). The salinity stress response function was defined in terms of the osmotic head (h_ϕ) according to Maas (1990). This stress response function requires two

parameters, i.e., the osmotic head threshold value ($h_{\phi\ threshold}$) corresponding to the value of h_ϕ above which root water uptake occurs without a reduction, and the slope (s) which determines the root water uptake decline per a unit decrease in the osmotic head below the threshold. Crop salinity tolerance data for the Maas (1990) function is usually tabulated in terms of the soil electrical conductivity of the saturation paste extract (EC_e) (Ayers and Westcot, 1985; Maas, 1990; Minhas et al., 2020). The conversion of the respective soil electrical conductivity threshold ($EC_{e\ threshold}$) and slope values to osmotic heads was carried out following Ramos et al. (2011). The effects of the water and salinity stresses were further assumed to be multiplicative (van Genuchten, 1987).

The partition of solutes between the liquid and solid phases in the Fickian-based convection–dispersion equation was described using exchange equations between the major cations Ca^{2+}, Mg^{2+}, Na^+, and K^+, and respective Gapon selectivity or exchange coefficients (White and Zelazny, Šimůnek and Suarez, Šimůnek et al., 1986, 1997, 2013):

$$K_{Mg/Ca} = \frac{\overline{Mg}^{2+}}{\overline{Ca}^{2+}} \quad \frac{\left(Ca^{2+}\right)^{0.5}}{\left(Mg^{2+}\right)^{0.5}} \tag{5}$$

$$K_{Ca/Na} = \frac{\overline{Ca}^{2+}}{\overline{Na}^{+}} \quad \frac{(Na^{+})}{\left(Ca^{2+}\right)^{0.5}} \tag{6}$$

$$K_{Ca/K} = \frac{\overline{Ca}^{2+}}{\bar{K}^{+}} \quad \frac{(\bar{K}^{+})}{\left(Ca^{2+}\right)^{0.5}} \tag{7}$$

where $K_{Mg/Ca}$, $K_{Ca/Na}$, and $K_{Ca/K}$ are the Gapon exchange constants (-) for the exchange reactions of calcium and magnesium, calcium and sodium, and calcium and potassium, respectively, in the liquid (Ca^{2+}, Mg^{2+}, Na^+, K^+) and solid phases ($\overline{Ca}^{2+}$, $\overline{Mg}^{2+}$, $\overline{Na}^{+}$, $\bar{K}^{+}$). This approach allows simulating aqueous complexation, salt precipitation/dissolution, and cation exchange reactions. The cation exchange capacity (CEC) is assumed as constant, given by the sum of the exchangeable cations ($\overline{Ca}^{2+}, \overline{Mg}^{2+}, \overline{Na}^{+}, \bar{K}^{+}$), and independent of pH (Šimůnek et al., 2013). Precipitation/dissolution reactions consider multicomponent kinetic expressions, which include both forward and back reactions. The Pitzer expressions are adopted for computing single ion activities (Šimůnek et al., 2013). The electrical conductivity of the soil solution (EC_{sw}) is determined from individual anions and cations following McNeal et al. (1970), while the sodium adsorption ratio (SAR) is computed from the simulated soluble Na^+, Ca^{2+}, Mg^{2+} concentrations according to the U.S. Salinity Laboratory Staff (1954) guidelines. Successful applications of the major ion chemistry module or UNSATCHEM module available in HYDRUS-1D can be found in Gonçalves et al. (2006), Ramos et al. (2011), Rasouli et al. (2013), Raij et al. (2016), and Phogat et al. (2020).

2.2.2. Model setup

In each of the nine studied orchards, the soil domain was defined as a one-dimensional column with 2.0 m depth discretized using 201 nodes. The soil was then divided into 4 layers, with depths of 0.0–0.2 m, 0.2–0.4 m, 0.4–0.6 m, 0.6–2.0 m, which were like this defined for calibration purposes. For the layers where information was available (Table 2), the soil hydraulic parameters were initially obtained by fitting the Mualem-van Genucthen model to measured soil hydraulic data. For the deeper layers, in which direct measurements of soil hydraulic properties were unavailable due to stoniness or inadequate soil moisture conditions for sampling undisturbed soil cores, the soil hydraulic parameters were defined using the pedotransfer functions (PTFs) in Ramos et al., (2013, 2014). Soil dispersivity (λ) values were initially estimated using PTFs in Gonçalves et al. (2002). The initial soil water contents were defined according to the measured data from capacitance probes at each location and depth at the beginning of each season. The initial concentration of Ca^{2+}, Mg^{2+}, Na^+, and K^+ in the liquid and solid phases were those presented in Table 3. Concentrations of soluble cations Na^+, Ca^{2+}, Mg^{2+}, and K^+ were measured in the soil solution collected from saturation extracts using atomic absorption spectrophotometry. Exchangeable cations $\overline{Ca}^{2+}, \overline{Mg}^{2+}, \overline{Na}^{+}, \bar{K}^{+}$ were determined with the Bascomb method (Bascomb, 1964) using a solution of $BaCl_2$ + Triethanolamine at pH 8.1. The concentration of Cl^- was calculated to maintain the charge balance, while the cation exchange capacity (CEC) was calculated from the sum of ion exchange species. The Gapon exchange constants were then computed from the initial solute conditions in the liquid and solid phases following Eqs. (5) through (7).

The upper boundary conditions were determined by the potential crop transpiration (T_c) and soil evaporation (E_s) rates, and the irrigation, rainfall, and concentration fluxes. T_c and E_s values were computed daily following the dual crop coefficient (dual-K_c) approach (Allen et al., 1998, 2005) using the SIMDualKc model (Rosa et al., 2012). This was fundamental for the accurate definition of surface boundary evapotranspiration fluxes in the study cases due to the great complexity associated with orchard systems. In these systems, surfaces are heterogenous, the soil is incompletely covered, and differences in the planting density, canopy height, training system, interrow management, and irrigation management influence the amount of energy available for both the transpiration and soil evaporation processes. All details on the application of the dual-K_c approach to the nine orchards can be found in the companion paper (Ramos et al., 2023). Root depth was defined according to observations, varying from 0.8 m in P3 and P5 to 1.0 m in the remaining sites. The bottom boundary condition was specified as free drainage.

T_c reductions due to water stress were computed for almond with the parameters defined in Phogat et al. (2018): $h_1 = -10$ cm, $h_2 = -25$ cm, $h_3 = -500$ to -800 cm, and $h_4 = -15{,}000$ cm. The salinity stress was computed with $h_{\phi\ threshold} = -1193.89$ cm and $s = 0.02499$ based on data tabulated in Minhas et al. (2020). For olive, the water stress was computed with the parameters defined in Egea et al. (2016): $h_1 = -10$ cm, $h_2 = -25$ cm, $h_3 = -3000$ to -5000 cm, and $h_4 = -18{,}000$ cm. The salinity stress used $h_{\phi\ threshold} = -3099.17$ cm and $s = 0.02099$ for the cv. Arbequina and Picual (Minhas et al., 2020), and $h_{\phi\ threshold} = -1579.94$ cm and $s = 0.02187$ for cv. Cobrançosa (Marin et al., 1985). For citrus: $h_1 = -10$ cm, $h_2 = -25$ cm, $h_3 = -200$ to -1000 cm, and $h_4 = -18{,}000$ cm (Šimůnek et al., 2013); and $h_{\phi\ threshold} = -1346.31$ cm and $s = 0.02099$ (Minhas et al., 2020). For pomegranate, the T_c reduction parameters due to water and salinity stresses were set identically to olive, thus assuming similar tolerance to drought and saline conditions.

2.2.3. Model calibration and validation

The HYDRUS-1D model was calibrated for each of the studied orchards using the 2019 dataset and validation was performed using the calibrated parameters with the 2020 dataset. Calibration procedures followed a two-step approach and were initiated by minimizing the deviation between measured and simulated soil moisture data. In a first step, the soil hydraulic parameters θ_s, α, and η were obtained through inverse modeling of daily soil water content data following Šimunek and van Genuchten (1996). The weighting coefficients used for the different soil water content data points in the objective function to be minimized were all assumed to be 1 since the observation errors of the measurements were unknown (Ramos et al., 2006; González et al., 2015). The θ_r was not modified as this parameter usually has little influence on simulated time series of soil water contents and soil pressure heads (González et al., 2015; Jacques et al., 2002; Šimůnek et al., 1998). The K_s was also not modified, being set to values measured in the laboratory when available or to the estimates provided by PTFs. This option was considered more realistic than the K_s values resulting from the inverse modeling procedure. The connectivity/tortuosity ℓ parameter was set to 0.5 following Mualem (1976). The statistical indicators used to evaluate the goodness-of-fit between observed and predicted soil water contents

Table 3
Initial concentrations of soluble ions and exchangeable cations in the different study sites.

Soil layer (m)	Soluble ions ($mmol_{(c)}\ l^{-1}$)					Exchangeable cations ($mmol_{(c)}\ kg^{-1}$)				CEC ($mmol_{(c)}\ kg^{-1}$)
	Ca^{2+}	Mg^{2+}	Na^{+}	K^{+}	Cl^{-}	$\overline{Ca}^{2+}$	$\overline{Mg}^{2+}$	$\overline{Na}^{+}$	$\overline{K}^{+}$	
P1. Almond										
0.0–0.2	0.23	0.18	0.67	0.10	1.18	9.50	6.71	1.52	0.92	18.65
0.2–0.4	0.40	0.63	0.77	0.01	1.81	24.73	22.50	1.81	0.27	49.31
0.4–0.6	0.28	0.79	1.12	0.02	2.21	25.45	38.05	4.52	0.35	68.37
0.6–2.0	0.04	0.25	1.39	0.02	1.70	53.17	114.74	8.22	0.60	176.73
P2. Almond										
0.0–0.2	0.13	0.19	0.83	0.07	1.22	21.66	11.45	1.38	0.90	35.39
0.2–0.4	0.09	0.14	0.91	0.02	1.16	66.56	75.01	4.46	0.69	146.72
0.4–0.6	0.04	0.1	1.04	0.02	1.20	132.58	206.66	13.35	0.74	353.33
0.6–2.0	0.09	0.46	2.54	0.01	3.10	128.38	166.68	20.01	0.07	315.14
P3. Olive										
0.0–0.2	0.32	0.20	0.49	0.04	1.05	16.69	4.27	0.85	1.13	22.94
0.2–0.4	0.17	0.15	0.42	0.09	0.83	15.61	3.83	0.83	1.59	21.86
0.4–0.6	0.43	0.31	0.51	0.05	1.30	15.49	6.16	1.53	0.90	24.08
0.6–2.0	0.44	0.48	0.56	0.02	1.50	21.91	15.24	2.55	1.02	40.72
P4. Olive										
0.0–0.2	0.32	0.21	0.41	0.31	1.25	42.89	2.82	0.53	1.92	48.16
0.2–0.4	0.19	0.16	0.38	0.16	0.89	40.59	8.51	0.93	1.50	51.53
0.4–0.6	0.06	0.12	0.34	0.01	0.53	38.29	14.2	1.32	1.08	54.89
0.6–2.0	0.14	0.44	0.90	0.03	1.51	33.99	22.32	1.80	1.25	59.36
P5. Olive										
0.0–0.2	2.02	0.22	0.33	0.01	2.58	393.72	30.16	1.58	3.77	429.23
0.2–0.4	1.50	0.15	0.51	0.01	2.17	409.26	29.16	1.65	1.60	441.67
0.4–2.0	1.06	0.30	0.66	0.01	2.03	250.43	34.48	1.60	0.52	287.03
P6. Orange										
0.0–0.6	1.14	0.59	2.46	0.01	4.20	24.81	10.58	1.22	2.30	38.91
0.6–2.0	0.15	0.19	2.03	0.01	2.38	102.67	44.77	7.73	1.28	156.46
P7. Clementine										
0.0–0.6	1.85	1.77	4.47	0.01	8.10	9.63	10.92	1.69	3.75	25.99
0.6–2.0	0.16	0.39	4.01	0.01	4.57	36.07	60.27	9.85	1.09	107.28
P8. Mandarin										
0.0–0.6	2.07	1.49	2.79	0.01	6.36	99.45	77.86	17.58	2.57	197.46
0.6–2.0	0.77	1.06	3.60	0.01	5.44	110.22	107.81	13.36	1.35	232.74
P9. Pomegranate										
0.0–0.2	0.30	0.55	0.64	1.21	2.70	15.41	12.11	1.09	6.03	34.64
0.2–0.4	0.08	0.14	0.71	0.16	1.09	14.11	11.8	2.25	2.59	30.75
0.4–0.6	0.04	0.06	0.76	0.03	0.89	12.16	14.55	1.13	0.51	28.35
0.6–2.0	0.02	0.16	2.23	0.05	2.46	50.45	73.99	9.98	0.8	135.22

were those recommended by Pereira et al. (2015): the regression coefficient of the linear regression through the origin (b_0); the coefficient of determination (R^2) of the ordinary least-squares regression between observed and predicted values; the mean absolute error (MAE); the root mean square error (RMSE); the ratio of the RMSE to the mean of the observed data (NRMSE); the percent bias of estimation (PBIAS); and the modeling efficiency (NSE).

Afterward soil moisture simulations were considered adequate, the soil dispersivity values and the Gapon exchange constants were calibrated in a second step following a trial-and-error procedure, i.e., by manually adjusting the referred parameters one at a time until deviations between model simulations and field measurements of the EC_e and SAR were minimized. The simulated EC_{sw} data were converted to EC_e for comparison with field data using the $EC_{sw}/EC_e = 2$ ratio (U.S. Salinity Laboratory Staff, 1954). Because field data were only periodically available providing insufficient data for some of the statistical indicators referred to above, the goodness-of-fit indicators used for assessing model performance were: b_0, MAE, RMSE, and NRMSE. This limitation of data was mainly due to the SARS-CoV-2 outbreak and restrictions imposed on traveling during the study period.

The full description of the statistical indicators can be found in Moriasi et al. (2007), Legates and McCabe (1999), and Nash and Sutcliffe (1970). In general, b_0 equal to 1 indicates that the predicted values are statistically identical to field measurements. R^2 values close to 1 show that the model can explain the variance of the observations. MAE, RMSE, and NRMSE values close to zero indicate that estimation errors are small and model predictions are good. In general, RMSE $\geq$ MAE. The degree to which the RMSE value exceeds the MAE is usually a good indicator of the presence and extent of outliers, or the variance of the differences between the modeled and observed values, which were here useful to assess considering that soil salinity can have other sources (e.g., fertigation) than that evaluated in the modeling approach (irrigation water quality). PBIAS values close to zero describe accurate model simulations, while negative or positive values indicate over- or under-estimation bias, respectively. NSE values close to 1 mean that model predictions are good since the residuals' variance is much smaller than the observed data variance. Contrarily, if NSE < 0, the observed mean is a better indicator than model predictions.

2.3. Irrigation scenarios

Soil salinization risks were accessed considering the inter-annual variability of weather conditions, the crop growing period, and irrigation needs during the period 1979–2020. The previously calibrated model parameters were naturally adopted as well as other settings. Soil salinization risks were determined from the cumulative data of the daily salt balance (SB; kg ha^{-1}) computed for each season as follows (Wilcox and Resch, 1963; Bresler et al., 1982):

$$SB = (TSC_{iw} + TSC_{rain}) - TSC_{dw} = 0.64[(D_{iw}EC_{iw} + D_{rain}EC_{rain}) - D_{dw}EC_{dw}]10 \quad (8)$$

where TSC_{iw}, TSC_{rain}, and TSC_{dw} are the total salt content of irrigation water, rainfall, and drainage water (kg ha^{-1}), respectively; D_{iw}, D_{rain}, and D_{dw} are the depth of irrigation water, rainfall, and drainage water (mm), respectively; and EC_{iw}, EC_{rain}, and EC_{dw} are the electrical

conductivity of irrigation water, rainfall, and drainage water (dS m^{-1}), respectively. The EC_{rain} was 0.10 dS m^{-1}, and this value was used for all salinity simulations. It is slightly below the value of 0.12 dS m^{-1} used by Phogat et al. (2018). The salt balance was computed for the 0.0–1.5 m soil layer. Positive values refer to salt accumulation in the root zone layer while negative values refer to the dominance of leaching from the same layer. For these scenarios, simulations were consecutively run from the beginning of one growing season to the day prior to the beginning of the next season so that leaching in the non-growing period could all be accounted for in the salt balance. For each case study, results of the salt balance for the period 1979–2020 were then sorted in ascending order, and the years corresponding to the probabilities of 20%, 50%, 80%, and 95% for non-exceedance were identified. For simplification purposes, these were assumed to represent humid, normal, dry, and very dry years, respectively.

For each study site, the ERA5 weather reanalysis data were used (Hersbach et al., 2018). This dataset provides several gridded meteorological parameters with an hourly timestep and a resolution of 0.28125° (31 km). The variables used were air and dewpoint temperatures at 2 m height (K), the u (longitude) and v (latitude) components of wind velocity at 10 m (u_{10}; m s^{-1}), solar radiation at the surface (J m^{-2}), and total rainfall (m). Weather hourly data was then converted to daily values. The u_{10} data was also converted to wind speed at 2 m height (u_2). The daily ET_o was computed using the FAO PM equation (Allen et al., 1978). The adequateness of using ERA5 for computing the incoming solar radiation and ET_o has been positively evaluated in a previous study by Paredes et al. (2021).

The surface boundary conditions in HYDRUS-1D, i.e., the daily T_p and E_p values as well as irrigation schedules for the 1979–2020 period were again estimated using the dual-K_c approach and the SIMDualKc model (Rosa et al., 2012). Details on the computation of crop irrigation needs for scenario analysis are provided in Ramos et al. (2023), which include the assumed initial conditions (measured values in 2019), the growing degree-days (GDD) observed during the monitored period (2019–2020) and used for defining the dates of each year's crop growth stages, the settings for irrigation triggering (imposing a crop water stress of 5%), and the pre-defined irrigation depths per event (5 mm). Mild deficit irrigation schedules were always adopted considering the limited water availability in the region, and that all studied crops can endure water deficit during most stages of their growth period without

Table 4
Calibrated model parameters.

Soil layer (m)	Soil hydraulic properties					λ (cm)	Gapon exchange constants		
	θ_r (cm^3 cm^{-3})	θ_s (cm^3 cm^{-3})	α (cm^{-1})	η (-)	K_s (cm d^{-1})		$K_{Ca/Mg}$	$K_{Ca/Na}$	$K_{Ca/K}$
P1. Almond									
0.0–0.2	0.065	0.468	0.003	1.506	172.2	15	0.798	0.390	0.104
0.2–0.4	0.065	0.336	0.002	1.464	75.5		0.725	0.744	0.049
0.4–0.6	0.095	0.325	0.002	1.709	70.1		0.890	0.533	0.036
0.6–2.0	0.068	0.330	0.004	1.434	70.1		0.863	2.010	0.011
P2. Almond									
0.0–0.2	0.065	0.392	0.003	1.672	90.8	10	0.434	1.622	0.039
0.2–0.4	0.065	0.349	0.003	1.691	90.8		0.907	2.059	0.016
0.4–0.6	0.095	0.295	0.006	1.500	70.5		0.955	2.381	0.006
0.6–2.0	0.068	0.295	0.006	1.472	70.5		0.574	2.427	0.001
P3. Olive									
0.0–0.2	0.065	0.332	0.001	1.487	73.4	20	0.323	1.700	0.130
0.2–0.4	0.065	0.300	0.001	1.472	73.4		0.260	1.800	0.099
0.4–0.6	0.065	0.318	0.002	1.473	77.8		0.468	1.300	0.126
0.6–2.0	0.065	0.398	0.002	1.696	80.8		0.664	1.300	0.158
P4. Olive									
0.0–0.2	0.065	0.355	0.001	1.593	83.8	15	0.081	2.610	0.033
0.2–0.4	0.065	0.300	0.001	1.524	83.8		0.225	1.693	0.028
0.4–0.6	0.065	0.300	0.001	1.648	77.3		0.255	1.863	0.039
0.6–2.0	0.065	0.300	0.001	1.800	80.8		0.378	1.992	0.057
P5. Olive									
0.0–0.2	0.100	0.502	0.007	1.142	500.0	65	2.231	15.769	0.096
0.2–0.4	0.100	0.463	0.002	1.163	1.2		2.226	15.873	0.034
0.4–0.6	0.068	0.413	0.001	1.045	500.0		2.260	8.396	0.015
0.6–2.0	0.068	0.430	0.004	1.030	126.1		2.260	8.396	0.015
P6. Orange									
0.0–0.2	0.065	0.351	0.121	1.060	451.0	45	0.593	2.094	0.699
0.2–0.4	0.065	0.325	0.001	1.670	451.0		0.593	2.094	0.699
0.4–0.6	0.065	0.328	0.008	1.261	451.0		0.593	2.094	0.699
0.6–2.0	0.065	0.320	0.005	1.301	81.8		0.385	3.130	0.034
P7. Clementine									
0.0–0.2	0.065	0.320	0.017	1.171	171.0	45	1.161	1.835	3.749
0.2–0.4	0.065	0.320	0.003	1.349	171.0		1.161	1.835	3.749
0.4–0.6	0.065	0.320	0.002	1.400	171.0		1.161	1.835	3.749
0.6–2.0	0.065	0.320	0.001	1.597	81.8		1.077	1.627	0.086
P8. Mandarin									
0.0–0.2	0.065	0.332	0.002	1.210	66.0	45	0.923	0.790	0.263
0.2–0.4	0.065	0.326	0.002	1.212	66.0		0.923	0.790	0.263
0.4–0.6	0.065	0.320	0.004	1.153	66.0		0.923	0.790	0.263
0.6–2.0	0.065	0.300	0.001	1.347	20.3		0.830	1.517	0.076
P9. Pomegranate									
0.0–0.2	0.065	0.357	0.002	1.474	132.5	45	0.584	2.732	0.139
0.2–0.4	0.065	0.426	0.004	1.386	132.5		0.636	2.708	0.090
0.4–0.6	0.065	0.340	0.002	1.391	132.5		0.882	2.968	0.035
0.6–2.0	0.065	0.300	0.002	1.393	87.1		0.462	6.977	0.006

Note: θ_r, residual water content; θ_s, saturated water content; α and η, empirical shape parameters; K_s, saturated hydraulic conductivity; λ, soil dispersivity; K, Gapon selectivity coefficient.

significantly affecting yields (Grattan et al., 2006; García-Tejero et al., 2012, 2018; Volschenk, 2020; Rallo et al., 2021).

3. Results and discussion

3.1. Model parametrization

Table 4 presents the model parameters calibrated during the 2019 growing season. The soil hydraulic parameters were in the range of those proposed by Ramos et al. (2013) for the different texture classes of soils in Portugal. Likewise, the soil dispersivity values found some agreement with those in Gonçalves et al. (2002) and Vanderborght and Vereecken (2007). Lastly, the Gapon exchange constants of medium-textured soils were close to values in Ramos et al. (2011) and Phogat (2018), while for fine-textured soils they were closer to values in Rasouli et al. (2013). The $K_{Ca/K}$ in the ridge layer (0.0–0.6 m) of site P7 was the exception, which value was found to be higher than those reported in the literature. Reasons for that result may be related with the soil characteristics.

3.2. Model performance

Fig. 3 shows, as an example, the measured soil water contents at 0.1, 0.3, 0.5, and 0.7 m depths and the respective HYDRUS-1D simulated values in the P1 orchard during the 2019 and 2020 growing seasons. The figures also include the depths and dates of irrigation and rainfall events. For orchards P2 to P8, the corresponding information can be found in Ramos et al. (2023) or in the supplementary material (Figs. S1 to S8). Similar to most of other case studies, soil water contents in P1 showed large variations along both growing seasons, with higher values usually observed during the rainfall season and lower values in the dry summer season when they were maintained only by drip irrigation. The exceptions were the citrus orchards (P6-P8), wherein soil water contents during the summer season were also generally high due to excessive applications of irrigation water as reported in the companion study (Ramos et al., 2023). In all plots, variations of soil water contents were further larger at shallower depths than in the deeper layers as a result of the small water depths used, root water uptake, water infiltration, and redistribution.

Table 5 presents the statistical indicators used to evaluate the goodness-of-fit between measured and simulated soil water contents in all case studies. For 2019 (the calibration year), the regression coefficients b_0 were all close to the 1.0 target, ranging from 0.975 (P4) to 1.011 (P8), indicating that the simulated values were close to the observed ones. The value of R^2 varied from 0.440 in P4 to 0.844 in P6, showing that the model could generally explain most of the variance of the observed data. The errors of the estimates were always small, with RMSE$\leq$ 0.022 cm^3 cm^{-3} and NRMSE$\leq$ 0.156. The PBIAS values were also quite small ($-1.149 \leq$PBIAS$\leq$0.845%), with no particular over- or under-estimation trend in simulating the measured data. Lastly, the NSE values were relatively high, ranging from 0.435 (P4) to 0.844 (P6), thus

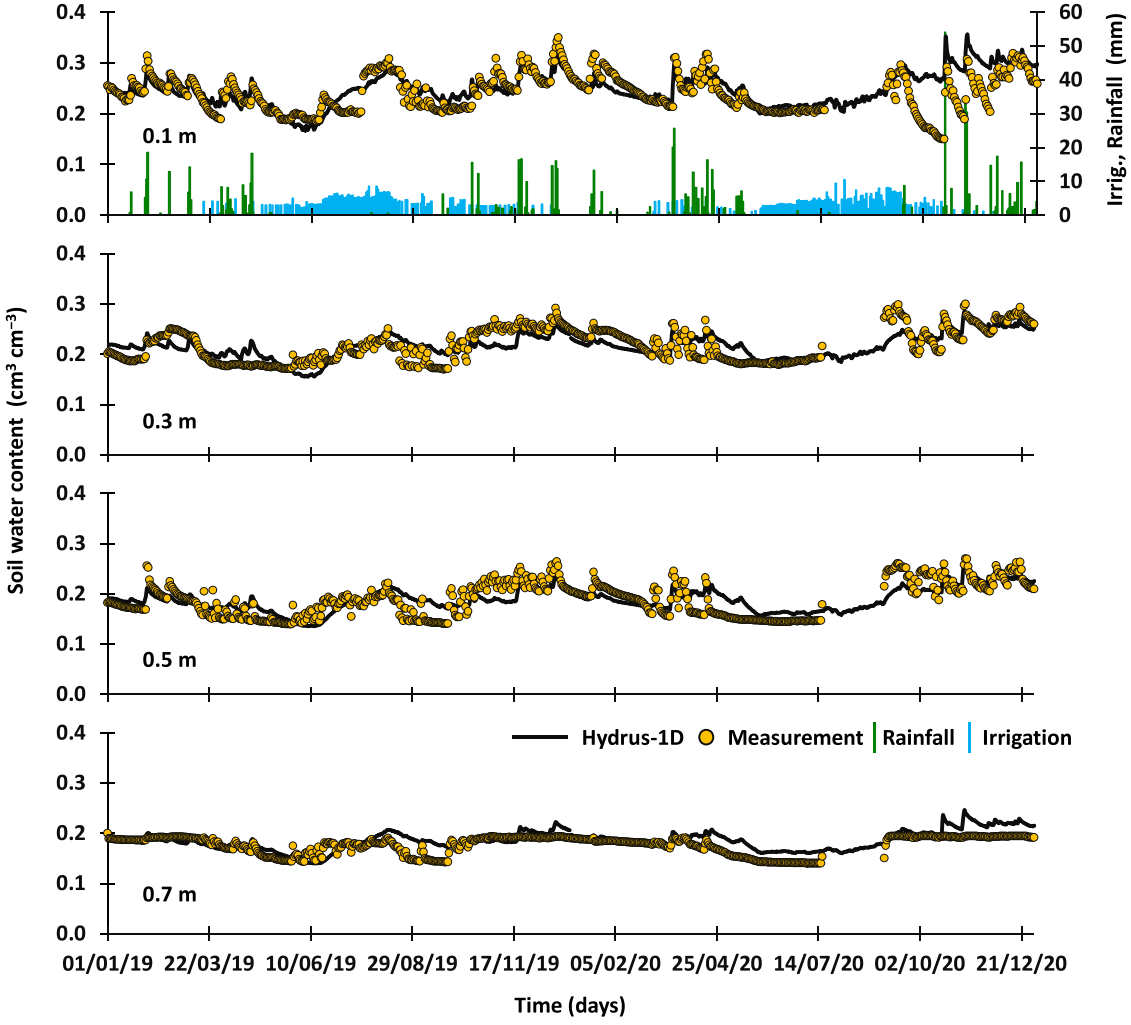

Fig. 3. Measured and simulated soil water contents at depths of 0.1, 0.3, 0.5, and 0.7 m and daily irrigation and rainfall depths in the P1 almond orchard during the 2019 and 2020 growing seasons.

Table 5
Goodness-of-fit indicators when comparing measured and HYDRUS-1D simulated soil water contents. Calibration and validations were performed with the 2019 and 2020 datasets, respectively.

Plot	b_0 (-)	R^2 (-)	MAE ($cm^3\ cm^{-3}$)	RMSE ($cm^3\ cm^{-3}$)	NRMSE (-)	PBIAS (%)	NSE (-)
P1. Almond							
2019	0.996	0.713	0.017	0.021	0.102	-0.604	0.712
2020	1.029	0.611	0.020	0.028	0.132	-4.148	0.552
P2. Almond							
2019	0.995	0.666	0.012	0.015	0.081	-0.039	0.659
2020	1.073	0.605	0.019	0.024	0.127	-7.791	0.237
P3. Olive							
2019	0.988	0.765	0.009	0.012	0.074	0.845	0.754
2020	1.051	0.719	0.013	0.017	0.096	-5.524	0.536
P4. Olive							
2019	0.975	0.440	0.016	0.021	0.156	0.425	0.435
2020	0.940	0.547	0.017	0.021	0.144	4.433	0.499
P5. Olive							
2019	0.998	0.740	0.015	0.022	0.057	-0.135	0.739
2020	1.009	0.644	0.016	0.023	0.057	-1.194	0.621
P6. Orange							
2019	0.993	0.844	0.014	0.019	0.078	0.074	0.844
2020	1.031	0.695	0.017	0.023	0.094	-3.299	0.549
P7. Clementine							
2019	1.001	0.768	0.008	0.011	0.062	-0.248	0.739
2020	1.009	0.725	0.010	0.013	0.070	-0.909	0.620
P8. Mandarin							
2019	1.011	0.770	0.009	0.012	0.048	-1.149	0.728
2020	1.006	0.736	0.010	0.012	0.046	-0.621	0.646
P9. Pomegranate							
2019	0.995	0.611	0.010	0.013	0.070	0.116	0.605
2020	0.986	0.604	0.012	0.017	0.084	0.898	0.587

Note: b_0, regression coefficient; R^2, coefficient of determination; MAE, mean absolute error; RMSE, root mean square error; NRMSE, ratio of the RMSE to the mean of observed data; PBIAS, percent bias; NSE, model efficiency.

indicating that the variance of the residuals was smaller than the measured data variance. For 2020 (the validation year), the goodness-of-fit indicators showed generally the same trend and a range of values similar to those observed at calibration. The worst statistics were obtained in P2 while the best indicators were in P8. Deviations between measured and simulated soil water content data may be explained by

Table 6
Goodness-of-fit indicators when comparing measured and simulated soil salinity. Calibration and validations were performed with the 2019 and 2020 datasets, respectively.

Field plot	EC_e				SAR			
	b_0 (-)	MAE ($dS\ m^{-1}$)	RMSE ($dS\ m^{-1}$)	NRMSE (-)	b_0 (-)	MAE $(mmol_{(c)}\ l^{-1})^{0.5}$	RMSE $(mmol_{(c)}\ l^{-1})^{0.5}$	NRMSE (-)
P1. Almond								
2019	0.295	1.627	2.322	0.892	0.718	0.705	0.845	0.334
2020	0.744	0.218	0.306	0.477	1.151	0.708	0.824	0.691
P2. Almond								
2019	1.131	0.244	0.291	0.302	0.900	0.821	1.043	0.591
2020	0.934	0.452	0.683	0.630	1.245	0.595	0.790	0.580
P3. Olive								
2019	0.314	0.998	1.283	0.842	0.680	0.900	1.102	0.392
2020	0.349	0.599	0.976	0.950	1.180	0.511	0.789	0.544
P4. Olive								
2019	0.455	0.545	0.940	0.979	0.570	0.783	1.024	0.553
2020	0.502	0.359	0.503	0.718	0.825	0.267	0.389	0.326
P5. Olive								
2019	0.466	0.360	0.479	0.634	0.667	0.667	0.824	0.411
2020	0.290	0.665	0.827	0.828	0.612	0.765	1.024	0.552
P6. Orange								
2019	0.431	0.482	0.939	0.809	0.793	0.629	1.048	0.388
2020	0.565	0.321	0.394	0.534	0.176	0.737	0.833	0.433
P7. Clementine								
2019	0.269	0.919	1.459	0.945	0.827	0.770	0.967	0.328
2020	0.534	0.348	0.508	0.609	1.045	0.625	0.775	0.340
P8. Mandarin								
2019	0.268	0.981	1.375	0.902	0.948	0.915	1.103	0.334
2020	0.596	0.288	0.727	0.790	1.099	0.868	1.045	0.461
P9. Pomegranate								
2019	0.459	0.908	1.763	0.830	1.063	0.858	1.057	0.361
2020	0.266	1.197	1.614	0.905	1.133	1.182	1.355	0.549

Note: EC_e, electrical conductivity of the soil saturation paste extract; SAR, sodium adsorption ratio; b_0, regression coefficient; MAE, mean absolute error; RMSE, root mean square error; NRMSE, ratio of the RMSE to the mean of observed data.

limitations in field data collection and representation of the three-dimensional drip irrigation system using a one-dimensional approach (Dabach et al., 2013; Ramos et al., 2012; Kandelous et al., 2011).

The goodness-of-fit between measured and simulated EC_e values was less good than that for soil moisture (Table 6). This was expected as solute transport simulations depend upon (i) soil moisture simulations; (ii) the assumed relationship for converting simulated EC_{sw} into EC_e, which is relatively straightforward but subjected to uncertainty (Skaggs et al., 2006a); and (iii) the less efficient trial-and-error calibration procedure used for solute transport parameters when compared with the inverse modeling approach used for soil hydraulic parameters. As shown in Fig. 4, there was an overall underestimation of the measured EC_e, namely for higher values. However, that underestimation was not observed for SAR, and thus for individual cations in the soil solution (Na^+, Ca^{2+}, and Mg^{2+}), where no tendency of under or over-prediction was noticed and pairwise comparisons of measurements and simulations aligned along the bisector of the scatterplot (Fig. 4).

The largest errors in EC_e simulations were found in P1, P7, and P8 in 2019, and P9 in both seasons (RMSE $\geq$ 1.375 dS m^{-1}). These correspond to plots where soil salinity reached the highest values, although causes were sometimes difficult to understand (Ramos et al., 2023). Thus, the differences between MAE and RMSE values were significant, indicating the presence of probable outliers (Table 6). In P1, soil salinity was attributed to fertigation events performed in 2019, with effects on soil salinity likely being transient and not noticed in 2020. In P7 and P8, soil salinity peaked only in December 2019, i.e., oddly during the rainfall season, with causes likely associated with unknown substances applied to anticipate/delay the maturation of fruits close to harvest. Farmers are often reluctant to provide information on fertilizers and phytopharmaceutical products applied to their crops, but related events show that the larger errors found in P1, P7, and P8 were related to causes other than poor modeling of the effects of irrigation water quality on soil salinity, such as missing information about fertigation events. In P9, in addition to the above mentioned causes, the poor drainage conditions of the Planosol soil may have not been well represented in the simulation domain, particularly at the bottom depths. As such, for the analysis that follows, one should consider that the salinity build-up due to fertigation events is not represented but, nonetheless, has some expression, particularly in intensive production orchards. Still, the overall performance of the model was considered appropriate for the analysis to follow.

3.3. Assessment of irrigation practices in the studied orchards

Table 7 presents the soil water balance computed by HYDRUS-1D for all case studies during the 2019 and 2020 growing seasons. As results are similar to those from SIMDualKc reported in the companion paper (Ramos et al., 2003), and the latter were extensively discussed, only a brief overview of HYDRUS-1D main results and of fundamental differences relative to the various plots are given herein.

In almond fields (P1 and P2), irrigation fulfilled most of the crop water needs during the irrigation season. Full irrigation or mild water deficits were noticed along the two growing seasons, with root water uptake reductions ranging from 1.2% to 10.3% of T_c values. Salinity stress was only found in P2 (2019), causing a mere reduction of T_c values of 3%. Contrarily to reported results in Ramos et al. (2023), no salinity stress was observed in P1 during the 2019 growing season, thus reflecting higher $T_{c\ act}$ and lower percolation values when compared with that reported SIMDualKc study. This was mainly due to the substantial conceptual differences between the two modeling approaches used for estimating the salinity stress. HYDRUS-1D simulations were not able to capture the impact of fertigation on soil salinity levels, particularly for this plot and season, producing thus some underestimation of its effects. SIMDualKc uses directly the EC_e measured in the field to compute the salinity stress and is therefore able to include such stress even if causes are not known.

In all other fields, SIMDualKc and HYDRUS-1D results were comparable. In olive fields (P3, P4, and P5), as typical of these systems, moderate water deficits were observed along the seasons, with root water uptake reductions of 4.0–23.6% of T_c values. In citrus fields (P6, P7, and P8), large percolation values (218–937 mm) were found due to excess irrigation and poor water management. In the pomegranate field (P9), no significant root water uptake reductions were noticed due to the high tolerance of this crop to drought and salinity.

The salt balance (Table 8) was much associated with irrigation management in each case study and seasonal rainfall. In 2019, when

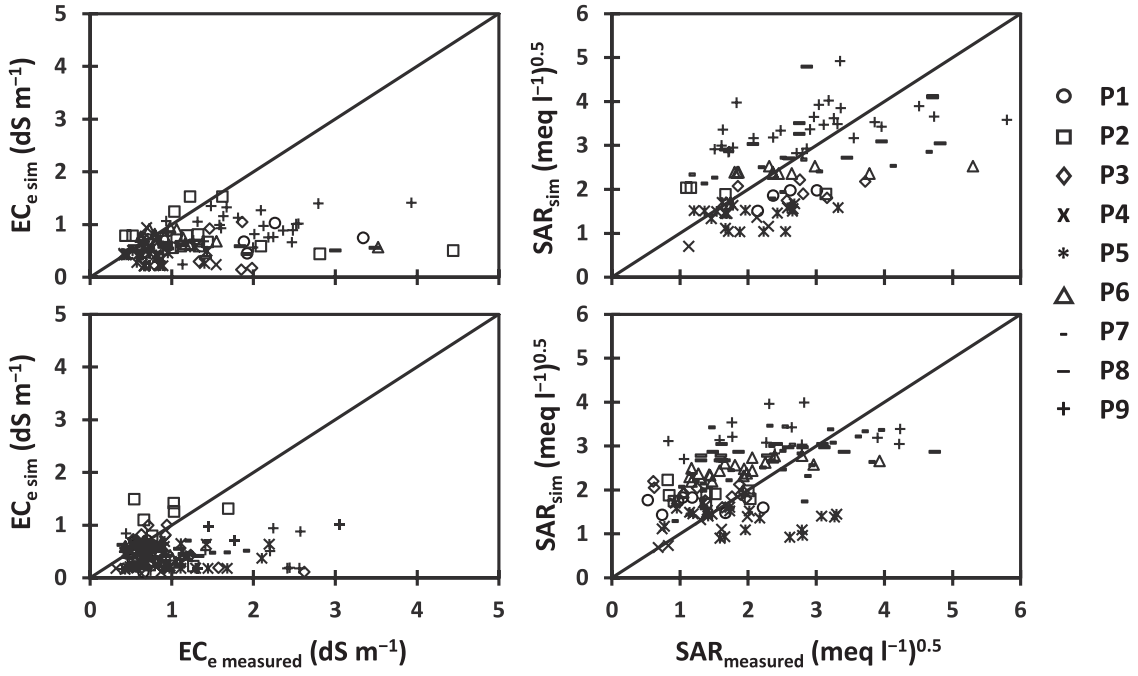

Fig. 4. Scatterplots of measured vs. simulated electrical conductivity of the soil saturated paste extract (EC_e) and sodium adsorption ratio (SAR) values in 2019 (top) and 2020 (bottom).

Table 7
Soil water balance in the study plots during the 2019 and 2020 seasons.

Plot	I (mm)	R (mm)	CR (mm)	ΔSW (mm)	T_c (mm)	$T_{c\ act}$ (mm)	E_s (mm)	DP (mm)	RO (mm)
P1. Almond									
2019	617	337	13	-27	661	593	232	109	6
2020	596	484	8	-33	656	601	225	205	24
P2. Almond									
2019	649	337	2	-1	660	621	247	113	6
2020	772	484	2	-16	656	648	237	337	20
P3. Olive									
2019	339	337	14	-57	431	385	195	40	10
2020	355	484	12	-61	427	425	204	121	38
P4. Olive									
2019	273	337	20	-32	433	316	200	60	18
2020	266	484	15	-12	428	355	226	121	50
P5. Olive									
2019	357	337	13	-48	445	337	192	117	14
2020	330	484	15	-10	440	401	215	158	47
P6. Orange									
2019	548	337	3	-18	516	491	161	218	27
2020	843	484	1	-18	510	442	241	609	27
P7. Clementine									
2019	653	337	1	-14	505	421	206	342	14
2020	858	484	1	-9	499	437	212	661	38
P8. Mandarin									
2019	906	337	4	-25	505	458	199	557	8
2020	1170	484	1	-4	499	473	220	937	27
P9. Pomegranate									
2019	654	337	16	-45	649	627	219	107	6
2020	694	484	10	-47	637	631	222	258	26

Note: I, irrigation; R, rainfall; CR, capillary rise; ΔSW, soil water storage variation; T_c, potential crop transpiration; $T_{c\ act}$, actual crop transpiration; E_s, soil evaporation; DP, deep percolation; RO, runoff.

Table 8
Salt balance in the study plots during the 2019 and 2020 seasons.

Field Plot	Inputs (tonnes ha^{-1})	Outputs (tonnes ha^{-1})	Balance (tonnes ha^{-1})
P1. Almond			
2019	3.06	0.86	2.20
2020	3.06	3.30	-0.24
P2. Almond			
2019	3.21	0.68	2.52
2020	3.87	6.36	-2.49
P3. Olive			
2019	1.78	0.23	1.55
2020	1.95	1.24	0.71
P4. Olive			
2019	1.47	0.30	1.18
2020	1.54	1.13	0.41
P5. Olive			
2019	1.86	0.79	1.08
2020	1.83	1.04	0.79
P6. Orange			
2019	2.74	3.23	-0.45
2020	4.17	9.58	-5.41
P7. Clementine			
2019	3.22	8.26	-5.03
2020	4.26	13.90	-9.64
P8. Mandarin			
2019	4.39	11.77	-7.34
2020	5.70	18.30	-12.56
P9. Pomegranate			
2019	3.23	1.72	1.51
2020	3.51	4.58	-1.08

season rainfall was below the mean average (337 mm), there was a general trend for salt accumulation in the soil profile, which was higher in almond (2.20 – 2.52 tonnes ha^{-1}) than in olive (1.08 – 1.55 tonnes ha^{-1}) or pomegranate (1.51 tonnes ha^{-1}) fields. The exceptions were the citrus fields (−0.45 to −7.34 tonnes ha^{-1}), where leaching dominated due to excessive irrigation. In 2020, when seasonal rainfall was above the mean annual average (484 mm), the salt balance became mostly negative in all plots, indicating leaching of salts by the end of the simulation period (December). Exceptions were again noticed, but this time in the olive fields where a small salt accumulation trend was noticed (0.41 – 0.79 tonnes ha^{-1}). Because deficit irrigation is practiced in these fields, thus percolation during the irrigation season is minimized, the amount of rainfall occurring in 2020 from October to December was not enough to leach salts away from the root zone layer. Results are thus in accordance with Dudley et al. (2008) and Ramos et al. (2019), referring to the risk of salt accumulation associated to deficit irrigation schedules.

3.4. Salinity build-up and climate variability

Table 9 presents the salt balance for the years corresponding to the probabilities of 20%, 50%, 80%, and 95% for non-exceedance, i.e., representing the humid, normal, dry, and very-dry years (determined with the simulations in the 1979–2020 period). However, factors influencing soil salinization were more diverse than meteorological conditions. Soil salinization risks were found to be site-specific and depending upon the seasonal irrigation and rainfall depths, the dates defining the crop stages, the rainfall distribution in the late and non-growing stages, and the soil drainage conditions, i.e., the soil hydraulic properties. Despite being an influencing factor, irrigation water quality was assumed constant throughout the 42 years of simulation, and a mild deficit irrigation strategy was also assumed for all crops and the simulation period.

In the P1 almond field, crop irrigation requirements ranged from 320 to 560 mm during the 1979–2020 period, while net rainfall varied from 279 to 705 mm. The resulting salt balance ranged from − 1.47–2.54 tonnes ha^{-1}, with negative values computed by the end of the season in 7 years (Fig. 5). Thus, P1 showed a probability of salt accumulation of 83.3% over a season (35 out of 42 years). In P2, irrigation requirements ranged from 335 to 575 mm. Net rainfall was close to P1, with small differences resulting from soil infiltration characteristics and runoff. The salt balance ranged from − 2.44–2.77 tonnes ha^{-1}, and the probability of salt accumulation over a season was 76.2%.

Table 9
Effect of climate variability on the salt balance in the soils of study sites.

Field plot	Humid year	Normal year	Dry year	Very-dry year
P1. Almond				
Net rainfall (mm)	570	428	331	340
Net irrigation (mm)	385	395	415	475
Salt balance (tonnes ha^{-1})	0.14	1.34	1.94	2.19
P2. Almond				
Net rainfall (mm)	583	431	418	343
Net irrigation (mm)	395	410	460	490
Salt balance (tonnes ha^{-1})	-0.32	1.42	1.96	2.23
P3. Olive				
Net rainfall (mm)	550	448	410	336
Net irrigation (mm)	390	360	475	490
Salt balance (tonnes ha^{-1})	0.06	1.25	2.02	2.35
P4. Olive				
Net rainfall (mm)	354	451	287	329
Net irrigation (mm)	530	340	415	490
Salt balance (tonnes ha^{-1})	-1.16	0.51	1.67	2.08
P5. Olive				
Net rainfall (mm)	454	426	336	307
Net irrigation (mm)	270	190	265	300
Salt balance (tonnes ha^{-1})	0.14	0.59	1.15	1.35
P6. Orange				
Net rainfall (mm)	397	455	317	294
Net irrigation (mm)	235	230	340	280
Salt balance (tonnes ha^{-1})	-1.48	-0.55	0.53	0.91
P7. Clementine				
Net rainfall (mm)	394	479	349	277
Net irrigation (mm)	220	280	315	355
Salt balance (tonnes ha^{-1})	-3.85	-2.93	-1.66	-1.13
P8. Mandarin				
Net rainfall (mm)	397	455	354	281
Net irrigation (mm)	215	215	315	355
Salt balance (tonnes ha^{-1})	-2.84	-1.76	-0.43	0.20
P9. Pomegranate				
Net rainfall (mm)	397	278	317	293
Net irrigation (mm)	340	575	450	400
Salt balance (tonnes ha^{-1})	-1.31	0.29	1.38	1.69

Hence, the risk of salinity build-up was slightly smaller in P2 than in P1, but still high.

The simulated EC_e reached higher values in P2 than in P1, which agrees with the monitoring period (2019–2020). Almond is sensitive to salinity, having an $EC_{e\ threshold}$ of 1.5 dS m^{-1} and a reduction of 19% in the growth rate for a unit increase in salinity beyond the threshold (Minhas et al., 2020). Salinity levels above the threshold during the cropping season could have a serious impact on growth and yields. In P1, EC_e values higher than the $EC_{e\ threshold}$ were predicted for the cases equaling or topping the probability of 95% for non-exceedance, i.e., very-dry years. In P1, $EC_e > EC_{e\ threshold}$ occurred only for a short period, by late September and below the 0.5 m soil depth. In P2, $EC_e > EC_{e\ threshold}$ for cases with a probability for non-exceedance $\geq$ 80%, i.e., dry and very-dry years, occurring by after the end of August, also at soil depths below 0.5 m. Because by then, on both cases, almond nuts are supposed to have been already harvested, controlling soil salinity by adding a leaching fraction to irrigation depths seems unneeded. However, in P2 and for seasons following very-dry periods, pre-season leaching may be required. In these very-dry seasons, EC_e values were maintained above the $EC_{e\ threshold}$ at deeper depths, increasing the risk of affecting the next season's flowering period, which occurs very early in the year (February). Rainfall during autumn and early winter may not be enough to leach salts accumulated during the previous irrigation season, with the risk of affecting the flowering stage. Simulations showed that applying 10–20 mm as pre-season irrigation (i.e., at the end of January) was enough to drop EC_e values below the $EC_{e\ threshold}$ in the rootzone layer by the beginning of the next growing season. Meanwhile, it should be assumed that when simulating drip irrigation in orchards using a two-dimensional model, the computed leaching may be less effective (Yang et al., 2019). Therefore, the required pre-season leaching irrigation depths may be higher than those predicted above. Nevertheless, transient state models such as HYDRUS-1D give a more accurate estimate of leaching needs than the traditional approach documented, for example, in Ayers and Westcot (1985), which many researchers believe to be conservative (Corwin et al., 2007; Letey et al., 2011; Corwin and Grattan, 2018).

In olive fields, irrigation needs ranged from 315 to 625 mm in P3, 285–630 mm in P4, and 175–410 mm in P5 during the 1979–2020 period. The salt balance varied from − 2.44–2.77 tonnes ha^{-1} in P3, − 4.09–2.53 tonnes ha^{-1} in P4, and − 1.0–1.60 tonnes ha^{-1} in P5 (Fig. 5). The probability of salt accumulation over a season was high in all fields, reaching 83.3% in P3, 64.3% in P4, and 81.0% in P5. Despite such high risks, soil salinity in P3 and P5 never reached harmful levels for plants. In these two locations, olive varieties (Arbequina and Picual) are moderately tolerant to salinity, and leaching during the rainfall period was always sufficient to control soil salinity levels even in the dry seasons. In P4, the olive variety (Cobrançosa) is more sensitive to soil salinity, at least when trees are young (Marin et al., 1995). The $EC_e > EC_{e\ threshold}$ occurred only for cases with probability for non-exceedance $\geq$ 97%, i.e., 2 years. In these years, adopting a leaching fraction by the beginning of September may be necessary to control soil salinity levels. For the year with the highest salt accumulation (2019), applying a leaching fraction of 30% after September 1st was sufficient to maintain $EC_e < EC_{e\ threshold}$, i.e., adding 1.5 mm per event, thus 40 mm of total irrigation water.

In citrus fields, irrigation requirements were relatively similar between the case studies, varying from 175 mm to 435 mm during the 1979–2020 period. The salt balance ranged from − 2.96–1.13 tonnes ha^{-1} in P6, − 5.69 to − 0.47 tonnes ha^{-1} in P7, and − 4.69–0.35 tonnes ha^{-1} in P8 (Fig. 5). The probability of salt accumulation over a season was only 28.7% in P6 and 7.1% in P8. In P7, the accumulation of salts at the end of a season was never detected. The $EC_e > EC_{e\ threshold}$ condition never occurred in any of these sites during the analyzed period. The citrus plots showed to have better drainage conditions than the almond and olive plots. The ridges where crops were planted likely played a decisive role on improving soil water flow conditions since the original soil profiles usually present poor drainage conditions.

Lastly, irrigation needs for pomegranate (P9) ranged from 290 to 575 mm, the salt balance varied from − 3.01–1.79 tonnes ha^{-1} (Fig. 5), and the probability of salt accumulation over a season was 64.3%. The simulations show that the crop was never affected by salinity stress as the tolerance threshold is relatively high ($EC_{e\ threshold}$ = 4 dS m^{-1}). Moreover, drainage conditions were improved as trees were also placed on ridges. Otherwise, crop development would likely be seriously affected by the poor drainage conditions of the Planosol soil.

To summarize, most of the study soils have high to very high risk tendency for accumulating salts from irrigation water over a growing season, namely during very dry years. However, for current climate conditions, adopting a mild deficit irrigation strategy and wide ridges, the risk of soil salinity levels reaching harmful levels to plants was very low. This conclusion was determined using a one-dimensional modeling approach but, in the study area, orchards are drip irrigated which implies caution in interpreting simulation results. In fact, salts tend to accumulate below the drippers, from where they are then transported downwards and sideways depending on irrigation volumes and frequency, rainfall, evapotranspiration rates, and soil hydraulic properties (Keller and Bliesner, 1990). One-dimensional representations of these systems can lead to inaccurate results in the short term, with the salinity build-up and the salinity stress in the root zone being most likely overestimated (Hanson et al., 2008), but such overestimation is not relevant in the current study since risks were, as referred above, very low. Furthermore, the salt balances were computed by the end of the leaching season, when salts are more evenly distributed in the soil profile, with their accumulation extending further than just below the drip emitter, thus approximating a one-dimensional solution (Ramos et al., 2012, 2019).

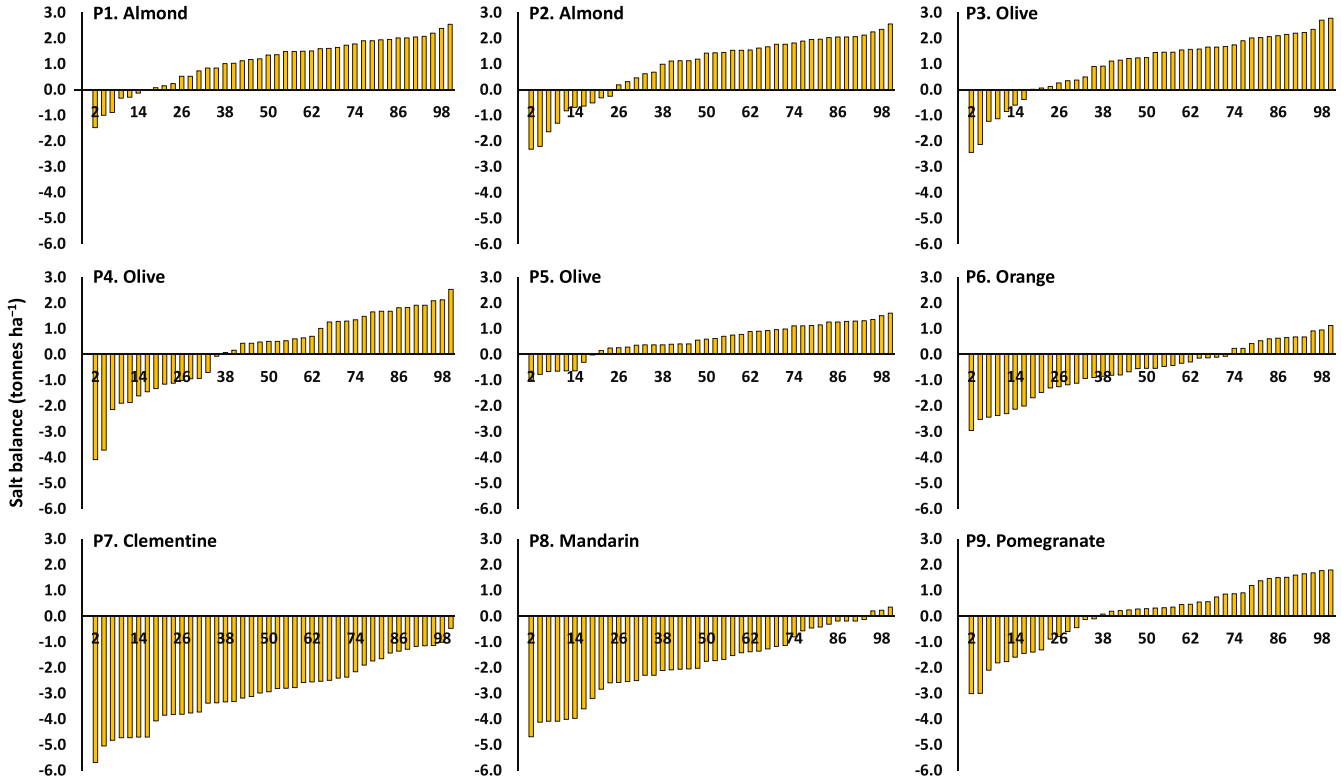

Fig. 5. Yearly salt balance in the nine case studies during the 1979–2020 period, sorted in ascending order (positive values refer to salt accumulation in the soil profile by the end of each growing season while negative values refer to the dominance of leaching).

4. Conclusions

The current paper presents and discusses soil salinization risks in nine commercial orchards in the Alentejo region, southern Portugal. The crops addressed are almond, olive, citrus (orange, clementine, and mandarin), and pomegranate. Soil water dynamics and salt transport were simulated in all cases using the major ion chemistry module in HYDRUS-1D. The model successfully simulated soil water contents measured in the different fields along two growing seasons, with small RMSE values ranging from 0.011 to 0.023 $cm^3\ cm^{-3}$. Simulations of the EC_e and SAR were more challenging, returning RMSE values varying from 0.291 to 2.322 dS m^{-1} and from 0.389 and 1.355 $(mmol_{(c)}\ l^{-1})^{0.5}$, respectively. There was a clear underestimation of the EC_e in some fields but simulations of SAR were quite acceptable. This shows that modeling errors were not associated with misrepresentations of the effects of irrigation water quality on soil salinity, but with other causes like missing information about fertigation events.

Soil salinization risks in the study sites were much associated with irrigation management and were site-specific. Factors like irrigation strategy, seasonal irrigation and rainfall depths, the crop growth season, the rainfall distribution in the late and non-growing stages, the soil drainage conditions, and the irrigation water quality were found to influence salt accumulation in the soil profile along the season. The risk of salt accumulation was high to very high for the very dry years in most studied orchards, with only the citrus plots being less prone to salinity build-up due to more favorable drainage conditions in the root zone domain and/or in the soil ridge where trees were planted. Nonetheless, for current climate conditions and irrigation water quality, the risk of soil salinity levels affecting crop development and yields was found to be minor. Rainfall leaching is sufficient to promote salt leaching during most seasons. Only in two of the study sites, it would be necessary to promote salt leaching during drier seasons following strategies that differed between locations. Notwithstanding, soil salinization risks can certainly be aggravated by fertilization management, which could not be simulated but was found to have a significant impact on soil salinity levels in some of the study sites. Climate change, which projections for the region include a significant decrease in rainfall, thus of the natural leaching process, may further aggravate soil salinization risks in the study areas, which should be object of future studies. Adopting a continuous monitoring of selected orchards may help to improve further studies and the support and dissemination of appropriate irrigation schedules and management.

Declaration of Competing Interest

The authors declare that they have no known competing financial interests or personal relationships that could have appeared to influence the work reported in this paper.

Data availability

Data will be made available on request.

Acknowledgments

This research project was funded by FCT/MCTES (PIDDAC) through project LARSyS–FCT Pluriannual funding 2020–2023 (UIDP/EEA/50009/2020), project SOIL4EVER (PTDC/ASP-SOL/28796/2017), and project HYDROVAR (2022.03921. PTDC). The support of FCT through grants attributed to T. B. Ramos (CEECIND/01152/2017) and H. Darouich (CEECIND/01153/2017) is also acknowledged.

Appendix A. Supporting information

Supplementary data associated with this article can be found in the online version at doi:10.1016/j.agwat.2023.108319.

References

Alexandre, C., Borralho, T., Durão, A., 2018. Evaluation of salinization and sodification in irrigated areas with limited soil data: case study in southern Portugal. Span. J. Soil Sci. 8, 102–120. https://doi.org/10.3232/SJSS.2018.V8.N1.07.

Allen, R.G., Pereira, L.S., Raes, D., Smith, M., 1998. Crop Evapotranspiration. Guidelines for Computing Crop Water Requirements, FAO Irrig. Drain. Paper 56. FAO, Rome, Italy, 300 pp.

Allen, R.G., Pereira, L.S., Smith, M., Raes, D., Wright, J.L., 2005. FAO-56 dual crop coefficient method for estimating evaporation from soil and application extensions. J. Irrig. Drain. Eng. 131 (1), 2–13. https://doi.org/10.1061/(ASCE)0733-9437(2005)131:1(2).

Ayers, R., Westcot, D., 1985. Water quality for agriculture. Irrig. Drain. Paper 29.FAO, Rome.

Bascomb, C.L., 1964. Rapid method for the determination of cation-exchange capacity of calcareous and non-calcareous soils. J. Sci. Food Agric. 12, 821–823. https://doi.org/10.1002/jsfa.2740151201.

Bresler, E., McNeal, B.L., Carter, D.L., 1982. Saline and Sodic Soils. Advanced Series in Agricultural Sciences 10. Springe -Verl. Berlim Heide 236.

Cameira, M.R., Pereira, A., Ahuja, L., Ma, L., 2014. Sustainability and environmental assessment of fertigation in an intensive olive grove under Mediterranean conditions. Agric. Water Manag. 146, 346–360. https://doi.org/10.1016/j.agwat.2014.09.007.

Conceição, N., Tezza, L., Häusler, M., Lourenço, S., Pacheco, C.A., Ferreira, M.I., 2017. Three years of monitoring evapotranspiration components and crop and stress coefficients in a deficit irrigated intensive olive orchard. Agric. Water Manag. 191, 138–152. https://doi.org/10.1016/j.agwat.2017.05.011.

Corwin, D.L., Grattan, S.R., 2018. Are existing irrigation salinity requirements guidelines overly conservative or obsolete. J. Irrig. Drain. Engr 144 (8), 02518001. https://doi.org/10.1061/(ASCE)IR.1943-4774.0001319.

Corwin, D.L., Rhoades, J.D., Šimůnek, J., 2007. Leaching requirements for soil salinity control: steady-state versus transient models. Agric. Water Manag. 90, 165–180. https://doi.org/10.1016/j.agwat.2007.02.007.

Dabach, S., Lazarovitch, N., Šimůnek, J., Shani, U., 2013. Numerical investigation of irrigation scheduling based on soil water status. Irrig. Sci. 31 (1), 27–36. https://doi.org/10.1007/s00271-011-0289-x.

Dudley, L.M., Ben-Gal, A., Lazarovitch, N., 2008. Drainage water reuse: biological, physical, and technological considerations for system management. J. Environ. Qual. 37, S25–S35. https://doi.org/10.2134/jeq2007.0314.

Egea, G., Diaz-Espejo, A., Fernández, J.E., 2016. Soil moisture dynamics in a hedgerow olive orchard under well-watered and deficit irrigation regimes: assessment, prediction and scenario analysis. Agric. Water Manag. 164, 197–211. https://doi.org/10.1016/j.agwat.2015.10.034.

Feddes, R.A., Kowalik, P.J., Zaradny, H. 1978. Simulation of field water use and crop yield. Simulation Monographs Pudoc., Wageningen, The Netherlands.

García-Tejero, I., Durán-Zuazo, V.H., Arriaga-Sevilla, J., Muriel Fernández, J.L., 2012. Impact of water stress on citrus yield. Agron. Sustain. Dev. 32, 651–659. https://doi.org/10.1007/s13593-011-0060-y.

García-Tejero, I., Moriana, A., Rodríguez Pleguezuelo, C.R., Durán Zuazo, V.H., Egea, G., 2018. Sustainable deficit-irrigation management in almonds (Prunus dulcis L.): different strategies to assess the crop water use. In: García-Tejero, I.F., Durán Zuazo, V.H. (Eds.), Water Scarcity and Sustainable Agriculture in Semiarid Environment, Chapter 12. Academic Press, pp. 271–298. https://doi.org/10.1016/B978-0-12-813164-0.00012-0.

Gonçalves, M.C., Leij, F.J., Schaap, M.G., 2002. Pedotransfer functions for solute transport parameters of Portuguese soils. Eur. J. Soil Sci. 52, 563–574. https://doi.org/10.1046/j.1365-2389.2001.00409.x.

Gonçalves, M.C., Šimůnek, J., Ramos, T.B., Martins, J.C., Neves, M.J., Pires, F.P., 2006. Multicomponent solute transport in soil lysimeters with waters of different quality. Water Resour. Res. 42, W08401. https://doi.org/10.1029/2005WR004802.

González, M.G., Ramos, T.B., Carlesso, R., Paredes, P., Petry, M.T., Martins, J.D., Aires, N.P., Pereira, L.S., 2015. Modelling soil water dynamics of full and deficit drip irrigated maize cultivated under a rain shelter. Biosyst. Eng. 132, 1–18. https://doi.org/10.1016/j.biosystemseng.2015.02.001.

Grattan, S.R., Berenguer, M.J., Connell, J.H., Polito, V.S., Vossen, P.M., 2006. Olive oil production as influenced by different quantities of applied water. Agric. Water Manag. 85, 133–140. https://doi.org/10.1016/j.agwat.2006.04.001.

Hanson, B.R., Šimůnek, J., Hopmans, J.W., 2008. Leaching with subsurface drip irrigation under saline, shallow ground water conditions. Vadose Zone J. 7, 810–818. https://doi.org/10.2136/vzj2007.0053.

Hersbach, H., Bell, B., Berrisford, P., Biavati, G., Horányi, A., Muñoz Sabater, J., Nicolas, J., Peubey, C., Radu, R., Rozum, I., Schepers, D., Simmons, A., Soci, C., Dee, D., Thépaut, J.-N., 2018. ERA5 hourly data on single levels from 1979 to present. Copernicus Climate Change Service (C3S) Climate Data Store (CDS). ⟨https://doi.org/10.24381/cds.adbb2d47⟩ (Last accessed 04–01-2022).

Hoffman, G.J., Shalhevet, J., 2007. Controlling salinity. In: Hoffman, G.J., Evans, R.G., Jensen, M.E., Martin, D.L., Elliot, R.L. (Eds.), Design and Operation of Farm Irrigation Systems, 2nd ed. ASABE, St. Joseph, MI, pp. 160–207.

Hopmans, J.W., Qureshi, A.S., Kisekka, I., Munns, R., Grattan, S.R., Rengasamy, P., Ben-Gal, A., Assouline, S., Javaux, M., Minhas, P.S., Raats, P.A.C., Skaggs, T.H., Wang, G., De Jong van Lier, Q., Jiao, H., Lavado, R.S., Lazarovitch, N., Li, B., Taleisnik, E., 2021. Critical knowledge gaps and research priorities in global soil salinity. Adv. Agron. 169, 1–191. https://doi.org/10.1016/bs.agron.2021.03.001.

IUSS Working Group W.R.B., 2014. World Reference Base for Soil Resources 2014. International Soil Classification System for Naming Soils and Creating Legends for Soil Maps. World Soil Resources Reports No. 106. FAO, Rome.

Jacques, D., Šimůnek, J., Timmerman, A., Feyen, J., 2002. Calibration of Richards' and convection-dispersion equations to field-scale water flow and solute transport under rainfall conditions. J. Hydrol. 259, 15–31. https://doi.org/10.1016/S0022-1694(01)00591-1.

Kandelous, M.M., Šimůnek, J., van Genuchten, M.Th, Malek, K., 2011. Soil water content distributions between two emitters of a subsurface drip irrigation system. Soil Sci. Soc. Am. J. 75 (2), 488497 https://doi.org/10.2136/sssaj2010.0181.

Keller, J., Bliesner, R.D., 1990. Sprinkle and Trickle Irrigation. Van Nostrand Reinhold, New York, p. 652.

Legates, D., McCabe, G., 1999. Evaluating the use of goodness of fit measures in hydrologic and hydroclimatic model validation. Water Resour. Res. 35, 233–241. https://doi.org/10.1029/1998WR900018.

Letey, J., Hoffman, G.J., Hopmans, J.W., Grattan, S.R., Suarez, D., Corwin, D.L., Oster, J.D., Wu, L., Amrhein, C., 2011. Evaluation of soil salinity leaching requirement guidelines. Agric. Water Manag. 98 (4), 502–506. https://doi.org/10.1016/j.agwat.2010.08.009.

Maas, E.V., 1990. Crop salt tolerance. In: Tanji, K.K. (Ed.), Agricultural Salinity Assessment and Management. Manual Eng. Pract, vol. 71. Am. Soc. of Civ. Eng., Reston, VA, pp. 262–304.

Marin, L., Benlloch, M., Fernández-Escobar, R., 1995. Screening of olive cultivars for salt tolerance. In: Sci. Hortic, 64, pp. 113–116. https://doi.org/10.1016/0304-4238(95)00832-6.

Martins, J.C., Vilar, M.T., Neves, M.J., Pires, F.P., Ramos, T.B., Prazeres, A.O., Gonçalves, M.C., 2005. Monitorização da salinidade e sodicidade de solos regados por rampas rotativas nos perímetros do Roxo e de Odivelas. Proceedings of the I National Congress of Irrigation and Drainage (CD-ROM), 5 to 8 of December. Centro Operativo e de Tecnologia do Regadio, Beja, Portugal.

McNeal, B.L., Oster, J.D., Hatcher, J.T., 1970. Calculation of electrical conductivity from solution composition data as an aid to in-situ estimation of soil salinity. Soil Sci. 110, 405–414. https://doi.org/10.1097/00010694-197012000-00008.

Minhas, P.S., Ramos, T.B., Ben-Gal, A., Pereira, L.S., 2020. Coping with salinity in irrigated agriculture: crop evapotranspiration and water management issues. Agric. Water Manag. 227, 105832 https://doi.org/10.1016/j.agwat.2019.105832.

Moriasi, D.N., Arnold, J.G., Van Liew, M.W., Bingner, R.L., Harmel, R.D., Veith, T.L., 2007. Model evaluation guidelines for systematic quantification of accuracy in watershed simulations. Trans. ASABE 50, 885–900. https://doi.org/10.13031/2013.23153.

Mualem, Y., 1976. A new model for predicting the hydraulic conductivity of unsaturated porous media. Water Resour. Res. 12, 513–522. https://doi.org/10.1029/WR012i003p00513.

Nash, J.E., Sutcliffe, J.V., 1970. River flow forecasting through conceptual models part I—A discussion of principles. J. Hydrol. 10, 282–290. https://doi.org/10.1016/0022-1694(70)90255-6.

Paço, T.A., Pôças, I., Cunha, M., Silvestre, J.C., Santos, F.L., Paredes, P., Pereira, L.S., 2014. Evapotranspiration and crop coefficients for a super intensive olive orchard. An application of SIMDualKc and METRIC models using ground and satellite observations. J. Hydrol. 519, 2067–2080. https://doi.org/10.1016/j.jhydrol.2014.09.075.

Paço, T.A., Paredes, P., Pereira, L.S., Silvestre, J., Santos, F.L., 2019. Crop coefficients and transpiration of a super intensive Arbequina olive orchard using the dual Kc approach and the Kcb computation with the fraction of ground cover and height. Water 11, 383. https://doi.org/10.3390/w11020383.

Paredes, P., Trigo, I., De Bruin, H., Simões, N., Pereira, L.S., 2021. Daily grass reference evapotranspiration with Meteosat Second Generation shortwave radiation and reference ET products. Agric. Water Manag. 248, 106543 https://doi.org/10.1016/j.agwat.2020.106543.

Pereira, L.S., Oweis, T., Zairi, A., 2002. Irrigation management under water scarcity. Agric. Water Manag. 57, 175–206. https://doi.org/10.1016/S0378-3774(02)00075-6.

Pereira, L.S., Cordery, I., Iacovides, I., 2009. Coping with Water scarcity. Addressing the Challenges. Springer, Dordrecht, p. 382.

Pereira, L.S., Duarte, E., Fragoso, R., 2014. Water use: recycling and desalination for agriculture. In: van Alfen, N. (Ed.), Encyclopedia of Agriculture and Food Systems, vol. 5. Elsevier, San Diego, pp. 407–424.

Pereira, L.S., Paredes, P., Rodrigues, G.C., Neves, M., 2015. Modeling malt barley water use and evapotranspiration partitioning in two contrasting rainfall years. Assessing AQUACROP and SIMDualKc models. Agric. Water Manag. 159, 239–254. https://doi.org/10.1016/j.agwat.2015.06.006.

Phogat, V., Pitt, T., Cox, J.W., Šimůnek, J., Skewes, M.A., 2018. Soil water and salinity dynamics under sprinkler irrigated almond exposed to a varied salinity stress at different growth stages. Agric. Water Manag. 201, 70–82. https://doi.org/10.1016/j.agwat.2018.01.018.

Phogat, V., Mallants, D., Cox, J.W., Šimůnek, J., Oliver, D.P., Pitt, T., Petrie, P.R., 2020. Impact of long-term recycled water irrigation on crop yield and soil chemical properties. Agric. Water Manag. 237, 106167 https://doi.org/10.1016/j.agwat.2020.106167.

Portela, M.M., Espinosa, L.A., Zelenakova, M., 2020. Long-term rainfall trends and their variability in mainland Portugal in the last 106 years. Climate 8, 146. https://doi.org/10.3390/cli8120146.

Raij, I., Šimůnek, J., Ben-Gal, A., Lazarovitch, N., 2016. Water flow and multicomponent solute transport in drip irrigated lysimeters: experiments and modeling. Water Resour. Res. 52, 6557–6574. https://doi.org/10.1002/2016WR018930.

Rallo, G., Paço, T.A., Paredes, P., Puig-Sirera, A., Massai, R., Provenzano, G., Pereira, L.S., 2021. Updated single and dual crop coefficients for tree and vine fruit crops. Agric. Water Manag. 250, 106645 http://dx.doi.org/33310.1016/j.agwat.2020.106645.

Ramos, T.B., Gonçalves, M.C., Martins, J.C., van Genuchten, M.T.H., Pires, F.P., 2006. Estimation of soil hydraulic properties from numerical inversion of tension disk infiltrometer data. Vadose Zone J. 5, 684–696. https://doi.org/10.2136/vzj2005.0076.

Ramos, T.B., Šimůnek, J., Gonçalves, M.C., Martins, J.C., Prazeres, A., Castanheira, N.L., Pereira, L.S., 2011. Field evaluation of a multicomponent solute transport model in soils irrigated with saline waters. J. Hydrol. 407, 129–144. https://doi.org/10.1016/j.jhydrol.2011.07.016.

Ramos, T.B., Šimůnek, J., Gonçalves, M.C., Martins, J.C., Prazeres, A., Pereira, L.S., 2012. Two-dimensional modeling of water and nitrogen fate from sweet sorghum irrigated with fresh and blended saline waters. Agric. Water Manag. 111, 87–104. https://doi.org/10.1016/j.agwat.2012.05.007.

Ramos, T.B., Gonçalves, M.C., Brito, D., Martins, J.C., Pereira, L.S., 2013. Development of class pedotransfer functions for integrating water retention properties into Portuguese soil maps. Soil Res 51, 262–277. https://doi.org/10.1071/SR12347.

Ramos, T.B., Gonçalves, M.C., Martins, J.C., Pereira, L.S., 2014. Comparação de diferentes funções de pedotransferência para estimar as propriedades hidráulicas dos solos em Portugal. In: Gonçalves, M.C., Ramos, T.B., Martins, J.C. (Eds.), Livro de Actas do Encontro Anual da Sociedade Portuguesa da Ciência do Solo, 26 to 28 June. Instituto Nacional de Investigação Agrária e Veterinária, Oeiras, pp. 29–34.

Ramos, T.B., Darouich, H., Šimůnek, J., Gonçalves, M.C., Martins, J.C., 2019. Soil salinization in very high-density olive orchards grown in southern Portugal: Current risks and possible trends. Agric. Water Manag. 217, 265–281. https://doi.org/10.1016/j.agwat.2019.02.047.

Ramos, T.B., Darouich, H., Oliveira, A.R., Farzamian, M., Monteiro, T., Castanheira, N., Paz, A., Gonçalves, M.C., Pereira, L.S., 2023. Water use and soil water balance of Mediterranean tree crops assessed with the SIMDualKc model in orchards of southern Portugal. Agric. Water Manag. 279, 108209 https://doi.org/10.1016/j.agwat.2023.108209.

Rasouli, F., Pouya, A.K., Šimůnek, J., 2013. Modeling the effects of saline water use in wheat-cultivated lands using the UNSATCHEM model. Irrig. Sci. 31, 1009–1024. https://doi.org/10.1007/s00271-012-0383-8.

Rhoades, J.D., Kandiah, A., Mashali, A.M., 1992. The use of saline water for crop production. Irrig. Drain. Pap. 48. FAO, Rome.

Rosa, R.D., Paredes, P., Rodrigues, G.C., Alves, I., Allen, R.G., Pereira, L.S., 2012. Implementing the dual crop coefficient approach in interactive software. 1. Background and computational strategy. Agric. Water Manag. 103, 8–24. https://doi.org/10.1016/j.agwat.2011.10.013.

Santos, F.L., 2018. Olive water use, crop coefficients, yield, and water productivity under two deficit irrigation strategies. Agronomy 8, 89. https://doi.org/10.3390/agronomy8060089.

Šimunek, J., van Genuchten, M.Th, 1996. Estimating unsaturated soil hydraulic properties from tension disc infiltrometer data by numerical inversion. Water Resour. Res. 32, 2683–2696. https://doi.org/10.1029/96WR01525.

Šimůnek, J., Hopmans, J.W., 2009. Modeling compensated root water and nutrient uptake. Ecol. Modell. 220, 505–521. https://doi.org/10.1016/j.ecolmodel.2008.11.004.

Šimůnek, J., Suarez, D.L., 1997. Sodic soil reclamation using multicomponent transport modeling. ASCE J. Irrig. Drain. Eng. 123 (5), 367–376. https://doi.org/10.1061/(ASCE)0733-9437(1997)123:5(367).

Šimůnek, J., Angulo-Jaramillo, R., Schaap, M.G., Vandervaere, J.P., van Genuchten, M. T., 1998. Using an inverse method to estimate the hydraulic properties of crusted soils from tension disc infiltrometer data. Geoderma 86, 61–81. https://doi.org/10.1016/S0016-7061(98)00035-4.

Šimůnek, J., Genuchten, M.Th, Šejna, M., 2008. Development and applications of the HYDRUS and STANMOD software packages and related codes. Vadose Zone J. 7 (2), 587–600. https://doi.org/10.2136/VZJ2007.0077.

Šimůnek, J., Šejna, M., Saito, H., Sakai, M., van Genuchten, M.Th., 2013. The HYDRUS-1D software package for simulating the one-dimensional movement of water, heat, and multiple solutes in variably-saturated media: Version 4.16.Dep. Environ. Sci., University of California, Riverside.

Šimůnek, J., van Genuchten, M.Th, Šejna, M., 2016. Recent developments and applications of the HYDRUS computer software packages. Vadose Zone J. 15 (7) https://doi.org/10.2136/vzj2016.04.0033.

Skaggs, T.H., Shouse, P.J., Poss, J.A., 2006a. Irrigating forage crops with saline waters: 2. Modeling root uptake and drainage. Vadose Zone J. 5, 824–837. https://doi.org/10.2136/vzj2005.0120.

Skaggs, T.H., van Genuchten, M.Th, Shouse, P.J., Poss, J.A., 2006b. Macroscopic approaches to root water uptake as a function of water and salinity stress. Agric. Water Manag. 86, 140–149. https://doi.org/10.1016/j.agwat.2006.06.005.

U.S. Salinity Laboratory Staff, 1954. Diagnosis and Improvement of Saline and Alcaly Soils. USDA Handbook 60. Washington, USA.

UNESCO, 2020. United Nations World Water Development Report 2020. Water and Climate Change, Paris, UNESCO.

van Genuchten, M.Th, 1980. A closed form equation for predicting the hydraulic conductivity of unsaturated soils. Soil Sci. Soc. Am. J. 44, 892–898. https://doi.org/10.2136/sssaj1980.03615995004400050002x.

van Genuchten, M.Th., 1987. A numerical model for water and solute movement in and below the root zone. Res. Rep. 121, U.S. Salinity Laboratory, USDA, ARS, Riverside, California.

Vanderborght, J., Vereecken, H., 2007. Review of dispersivities for transport modeling in soils. Vadose Zone J. 6, 29–52. https://doi.org/10.2136/vzj2006.0096.

Volschenk, T., 2020. Water use and irrigation management of pomegranate trees - A review. Agric. Water Manag. 241, 106375 https://doi.org/10.1016/j.agwat.2020.106375.

White, N.L., Zelazny, L.M., 1986. Charge properties in soil colloids. In: Sparks, D.L. (Ed.), Soil Physical Chemistry. CRC Press, Boca Raton, Flo, pp. 39–81.

Wilcox, L.V., Resch, W.F., 1963. Salt balance and leaching requirements in irrigated lands. USDA, pp. 1290 Tech. Bul.

Yang, T., Šimůnek, J., Mo, M., Mccullough-Sanden, B., Shahrokhnia, H., Cherchian, S., Wu, L., 2019. Assessing salinity leaching efficiency in three soils by the HYDRUS-1D and -2D simulations. Soil . Res. 194, 104342 https://doi.org/10.1016/j.still.2019.104342.